AIAA JOURNAL
Vol. 47, No. 6, June 2009

Unsteady Flamelet Response in the Near Field of High-Reynolds-Number Jets

Rishikesh Venugopal* and John Abraham†
Purdue University, West Lafayette, Indiana 47907

DOI: 10.2514/1.40153

In this work, we perform numerical studies of the unsteady response of laminar diffusion flamelets relevant to the near field ($x/d < 30$) of high-Reynolds-number gaseous-fuel jets that are injected into high-pressure and high-temperature chambers. A large-eddy simulation database of a 70,000-Reynolds-number variable-density round jet is employed to compute turbulent time histories of the scalar dissipation rate in the near field. With this information, studies of diffusion flamelets subjected to scalar dissipation rate fluctuations are performed in which the unsteady flamelet equations are solved with the assumption of unity species Lewis number. The commonly employed diesel fuel surrogate *n*-heptane is chosen as the fuel, and its oxidation chemistry is modeled by a kinetic mechanism incorporating 159 species among 1540 reaction steps. Results show that in the simulated near field of the 70,000-Reynolds-number jet, transient temporary flame-weakening events followed by flame recovery are probable. Although the flame temperature, major species, and pollutants such as unburned hydrocarbons show a relatively fast response and good agreement with steady flamelet predictions, the pollutant, nitric oxide, responds with a significant phase lag, rendering steady flamelets inadequate. The analysis is extrapolated to higher-Reynolds-number jets with higher-intensity scalar dissipation rate fluctuations, in which transient flame-extinction/reignition events are observed. The applicability of steady flamelets to predict temperature and species responses during extinction/reignition is assessed, and the implications of extinction/reignition events for jet near-field phenomena, such as flame liftoff, are explored.

Nomenclature

c	=	progress variable
h	=	specific sensible enthalpy of the mixture
h_k^0	=	standard enthalpy of formation of species k
p	=	pressure
T	=	temperature
$\dot{w}_k$	=	chemical production/destruction rate of species k
Y_k	=	mass fraction of the kth species
Z	=	mixture fraction
ρ	=	mass density of the mixture
χ	=	instantaneous scalar dissipation rate
χ_e	=	steady extinction limit for a laminar diffusion flamelet
χ_{st}	=	conditional-mean scalar dissipation rate conditioned on the stoichiometric mixture fraction

I. Introduction

TURBULENT jet flames are inherently unsteady and are characterized by spatiotemporal fluctuations of quantities, such as the flame temperature, species concentrations, and mixing and reaction rates. Fluctuations arising from turbulence–chemistry interactions [1,2] may be particularly significant in the near field of jet flames, in which they can influence phenomena such as flame liftoff [1]. For instance, in the case of diesel jet flames, recent experiments [3,4] have shown that liftoff not only controls flame stabilization, but also the formation of pollutants such as soot through fuel–air premixing in the near field. Conventional modeling approaches employing Reynolds-averaged Navier–Stokes (RANS)-based closures, such as steady flamelet models [5] and perfectly stirred reactors [6], have been successful in the prediction of steady flame liftoff over a limited range of conditions. These models, however, are not able to predict transient variations in the liftoff height [7]; this limitation may arise from the neglect of effects due to flow unsteadiness on the local and transient flame structure. Hence, it is important to assess the applicability of commonly employed closures, such as steady flamelets, in the jet near field and to assess the potential impact of unsteady effects on jet near-field phenomena, such as flame liftoff.

In the near field of the jet in which liftoff occurs, turbulence–chemistry interactions can influence a variety of processes, such as autoignition [1,8], partially premixed flame propagation [1,9], and local extinction/reignition [1,9]. For instance, consider one possible conceptual picture of the instantaneous flowfield of a lifted-jet diffusion flame, shown in Fig. 1. As shown in the figure, autoignition kernels that originate downstream in the jet may propagate upstream and undergo local extinction/reignition at the base of the lifted-jet flame. Although unsteady effects on all of these contributing phenomena such as autoignition, flame propagation, and extinction/reignition are important, we focus on extinction/reignition in this work. Consistent with the laminar flamelet concept for turbulent jet flames [1], we investigate the unsteady response of laminar diffusion flamelets subject to fluctuations of the scalar dissipation rate.

The approach adopted in this work is as follows. Turbulent time records of the scalar dissipation rate are obtained from the analysis of the near field of a nonreacting, 70,000-Reynolds-number, variable-density, round gaseous-fuel jet computed with large-eddy simulation (LES). With this information, the unsteady response of flamelets (i.e., flame temperature, major species, and pollutants computed with the flamelet assumption) are investigated and the applicability of steady flamelet libraries is assessed. The analysis is extrapolated to jets with higher global strain rates, in which local extinction/reignition events may be observed, and the potential impact of extinction/reignition events on flame liftoff is discussed.

Note that neglecting the effects of combustion heat release on the predicted scalar dissipation rates in the LES is an important simplification in our approach. There are only few studies in the literature focusing on the effects of heat release on passive scalar statistics and scalar dissipation rates. For instance, recent direct numerical simulation (DNS) studies of Pantano et al. [10] in reacting

Received 30 July 2008; revision received 31 January 2009; accepted for publication 9 February 2009.

*Graduate Research Assistant, School of Mechanical Engineering, 500 Allison Road. Student Member AIAA.

†Professor, School of Mechanical Engineering, 500 Allison Road. Senior Member AIAA.

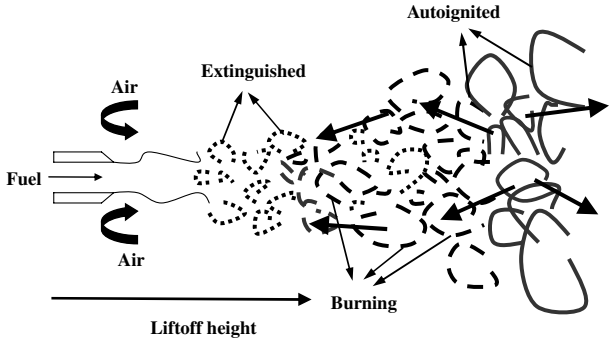

Fig. 1 Conceptual picture of the instantaneous flowfield of a lifted-jet diffusion flame.

mixing layers show that turbulent kinetic energies and turbulent dissipation rates, as well as scalar variances and dissipation rates, show a moderate sensitivity to heat release. The authors found that whereas the peak values of the scalar dissipation rate in reacting mixing layers decrease by up to 30% relative to nonreacting mixing layers, reacting mixing layers with different levels of heat release show minor differences. On the other hand, recent LES studies and experiments of Geyer et al. [11] in turbulent opposed-flow jets show that combustion heat release increases scalar dissipation rate magnitudes due to increased diffusivities. Although the effects of heat release on scalar statistics in high-Reynolds-number jets are not known to our best knowledge, it is likely that χ_{st} amplitudes in the generated flamelet histories would be affected. However, the DNS of Pantano et al. [10] in reacting shear layers and the LES studies of Pitsch and Steiner [12] in reacting jets show that probability density functions (PDFs) of conditional-mean scalar dissipation rates (i.e., χ_{st}) show lognormality, just as in the case of nonreacting jets. Hence, it is expected that the nature of fluctuations of χ_{st} computed in the present case for the near field of a nonreacting jet is fairly representative of the fluctuations in the presence of heat release and reaction zones, even though magnitudes encountered are likely to differ. In addition, with respect to jet near-field phenomena, such as flame liftoff, it is well known that theories entirely based on the large-scale mixing behavior of isothermal jets [13,14] have met with reasonable success in qualitatively and quantitatively predicting experimental trends [14].

It is realized that an alternative to account for combustion heat release effects on scalar dissipation rates is to carry out LES with relatively simple models, such as steady flamelets or equilibrium chemistry models. However, such simple models are likely to yield erroneous effects of heat release on the mixing field, which may further affect the conclusions drawn from this work. Moreover, the present nonreacting LES jet is amenable to validation through comparisons with readily available data on passive scalar statistics in self-similar jets [15–18]. The absence of such measured data for validation in the case of reacting jets would further increase the numerical uncertainties in the analysis. Nevertheless, the influence of heat release on scalar dissipation rates in the near field of high-Reynolds-number jets has to be clarified in future experimental and computational investigations.

Comprehensive reviews of LES of nonreacting and reacting flows may be found in several publications [19–21]. Recent studies have focused on velocity field statistics in nonreacting high-Reynolds-number jets [22,23] and passive scalar statistics in nonreacting low-Reynolds-number jets [24]. The LES studies of high-Reynolds-number variable-density jets, typical of diesel engine applications, are limited in the literature. In the present work, we employ the LES formulation recently employed by Anders et al. [25] to compute passive scalar statistics and turbulent time histories of scalar dissipation rates in the near field ($x/d < 30$) of a 70,000-Reynolds-number jet with an injected-to-ambient gas density ratio of 3.5. Next, we will briefly discuss previous works in the literature that focus on the unsteady response of diffusion flames.

The effect of flow unsteadiness on the structure of counterflow diffusion flames has received considerable attention in the last two decades [26–30]. These studies have been carried out by imposing oscillatory strain rates on the flames. Two major conclusions from these studies are as follows:

1) At high frequencies of the imposed perturbation, the flame becomes relatively insensitive due to increased phase lag.

2) This insensitivity may lead to extinction strain rates higher than steady limits.

Egolfopoulos and Campbell [26] performed numerical investigations of counterflow methane–air flames subject to velocity and fuel mass-fraction oscillations at the nozzle exits. It was shown that the phase lag associated with the flame response at high frequencies results from the attenuation of the oscillations imposed in the outer convective layer, by diffusion in the inner diffusive-reactive layer. In other words, the unsteady response of diffusion flames is diffusion-limited. In another numerical study involving counterflow methane–air flames, Im et al. [27] investigated the chemical response of species including pollutants such as carbon monoxide (CO) and nitrogen oxides (NO_x) to oscillating strain rate under conditions far from extinction. Their studies showed that owing to relatively slow characteristic chemical time scales, the response of CO and NO_x is weak at high frequencies. Furthermore, the authors showed that the scalar dissipation rate χ is a more appropriate parameter to characterize unsteady flames than the strain rate, because χ accounts for the diffusion-limited flame response. In this context, the present study employs the flamelet formulation, where χ directly appears as a parameter incorporating the flow unsteadiness. Note that in addition to the numerical works discussed previously, recent experiments [28] on propane–air diffusion flames have also confirmed the diffusion-limited frequency response of diffusion flames to strain rate oscillations, resulting in an increased lag at high frequencies.

Oscillatory perturbation studies have also focused on unsteady flame extinction. For instance, Im et al. [29] compared the unsteady response of near-extinction flames and flames in the Burke–Schumann limit (i.e., infinitely fast chemistry). Near-extinction flames were shown to be more sensitive to flow unsteadiness, and the heat release rate response of these flames exhibited a phase lag to the imposed strain rate oscillation. Unsteady extinction in counterflow hydrogen–air flames in the presence of sinusoidal strain was studied numerically and experimentally by Kistler et al. [30]. These studies showed that for strongly burning flames (i.e., flames initially far from extinction), the unsteady extinction strain rates increasingly deviate from steady values at relatively high frequencies, due to the delayed response of the flames. In addition to oscillatory strain rate studies, unsteady effects on diffusion flames have received attention through studies of flame–vortex interactions [31–33]. In agreement with the oscillatory perturbation studies, the flame–vortex interaction studies [32,33] indicate that unsteady extinction limits may be higher than steady values and that the unsteady limits are flow-dependent (i.e., increase with an increase in the vortex velocity scale).

Although the studies discussed previously employing oscillatory or vortex-induced perturbations have provided useful insight into the unsteady response of diffusion flames, they only include the effects due to a specific amplitude and frequency (i.e., due to a single turbulent eddy). In a turbulent jet flame, the flamelets would continuously interact with a spectrum of eddies (i.e., amplitudes and frequencies), which may alter the unsteady flame response and the probabilities of events such as local extinction. Hence, in this work, we focus on the more realistic case of flamelets subjected to turbulent fluctuations of the scalar dissipation rate χ. Note that studies focusing on the unsteady flame response to χ fluctuations are limited in the literature. Recent reacting LES studies of Pitsch [34] investigated the role of locally resolved fluctuations of χ to the predictions of the mean flame structure of Sandia flame D [35]. Predictions from two flamelet models, one accounting only for the conditionally averaged χ and the other accounting for locally resolved fluctuations of χ, were compared with experimental data. It was shown that accounting for local fluctuations of χ resulted in improved predictions, particularly for intermediates such as CO and H_2 and pollutants such as NO. Though the unsteady responses of the flame temperature and species were not investigated in detail, it was argued that modeling

unsteady effects on the turbulence–chemistry interactions resulted in improved predictions.

In a turbulent jet flame, excursions of the instantaneous scalar dissipation rate χ greater than or equal to the steady extinction limit χ_e [1,36] may lead to local extinction events. Following local extinction, the extinguished flamelets may reignite through one or more means, such as autoignition [37] or edge-flame dynamics [33,37,38]. In recent years, reignition phenomena have received attention through experimental works on vortex-perturbed flames [39,40], and numerical works in reacting isotropic turbulence [37], flame–vortex interactions [33,38,41], and jet flames [42,43]. The studies of Sripakagorn et al. [37] in reacting isotropic turbulence and those of Venugopal and Abraham [33,38] in vortex-perturbed flames show that mechanisms such as edge-flame propagation are more likely to cause reignition than autoignition when the excursions of χ above χ_e are large. In this work, the choice of the flamelet formulation precludes the inclusion of edge-flame-related phenomena, which are governed by curvature effects [33,38], so that the reignition phenomena reported in this work occur only through autoignition. Nevertheless, studies so far have not focused on the unsteady response of the flame temperature, major species, and pollutants during extinction/reignition events. In this context, our work provides insight into unsteady extinction and reignition through autoignition, which is one of the possible reignition scenarios in a turbulent jet flame. Moreover, note that although previous works have focused on simpler fuels such as methane, we choose *n*-heptane as the fuel, which is a commonly used surrogate for practical fuels such as diesel. A more complex fuel such as *n*-heptane has a wider range of chemical time scales that may interact with the flow unsteadiness.

In the following section, we outline the specific objectives and contributions of this work. Thereafter, the numerical formulation is presented in Sec. III. Results and discussion follow in Sec. IV. The paper closes with conclusions in Sec. V.

II. Objectives and Contributions

In this work, we are interested in the unsteady response of laminar diffusion flamelets subjected to turbulent fluctuations of the scalar dissipation rate χ. These turbulent fluctuations of χ are obtained from the analysis of the near field of a 70,000-Reynolds-number variable-density round gas jet computed using LES. The following questions are addressed in the present work:

1) How do diffusion flamelets (specifically, the temperature and species) respond to turbulent fluctuations of χ representative of the near field of variable-density high-Reynolds-number jets?

2) Are steady flamelets applicable for the predictions of the temperature and species responses in unsteady flowfields?

3) What is the impact of extinction/reignition events on the unsteady flame response, and the applicability of steady flamelets?

4) What are the implications of extinction/reignition events for flame liftoff in high-Reynolds-number jets?

In our opinion, the preceding questions have not been addressed adequately in the literature, but they are important for the understanding of localized flame dynamics in high-Reynolds-number jet flames commonly encountered in applications, such as diesel engines and gas turbines. We employ a higher hydrocarbon, *n*-heptane, as the fuel to represent practical fuels such as diesel. Relatively high pressures (40 bar) and high oxidizer temperatures (1000 K) are employed. Part of the motivation for using high pressures and temperatures is to capture reignition through autoignition following extinction, which can be described within the framework of flamelet modeling.

III. Numerical Formulation

A. LES

The Flow, Large-Eddy and Direct Simulation (FLEDS) code [25,44,45] is employed for the LES of a 70,000-Reynolds-number variable-density isothermal round gaseous-fuel jet. The FLEDS code has been employed in previous DNS studies of nonreacting mixing layers [44] and reacting jets [45], LES of nonreacting jets [25], and studies of flame–vortex interactions [33,38]. A detailed discussion of the LES formulation employed here, including the numerical schemes, filter characteristics, subgrid-scale models, and inlet-perturbation techniques, may be found in a recent publication by Anders et al. [25]. Here, we will present only a brief summary.

Spatial discretization is achieved through the sixth-order compact finite-difference scheme of Lele [46], and a compact-storage fourth-order Runge–Kutta scheme [47] is employed for time integration. A sixth-order tridiagonal filter [46] is implemented for spatial filtering. Subsonic inflow and partially reflecting outflow characteristic boundary conditions [48] extended for multicomponent gaseous mixtures [25] are employed. To trigger transition to turbulence, the vortex-ring perturbation technique of Bogey et al. [23] is used. In addition, a numerical-sponge layer is implemented [49] to suppress turbulent fluctuations and spurious pressure waves at the exit boundary that could lead to numerical instabilities and contamination of the physical jet flowfield. In the sponge layer, artificial damping terms are added to gradually transition the flowfield to a smooth target solution, which is chosen in the present case as the self-similar solution for an incompressible round jet [50]. The compressible form of the constant-coefficient Smagorinsky model [25] is employed for subscale closure.

The center z–x plane of the 3-D numerical grid is shown in Fig. 2. The physical region of the grid in which the jet flowfield of interest is simulated extends up to 25 jet diameters in the axial direction. Beyond this distance, a sponge region is implemented with exponential grid stretching and artificial damping. The 3-D grid comprises 401 (axial) $\times$ 113 $\times$ 113 grid points, which leads to a total of about 5.1 million points. The simulated jet exit Reynolds number is about 70,000 and the exit diameter d is 1 mm. As indicated in Fig. 2, the physical part of the domain has 351 points in the axial direction. This results in a uniform resolution of about 71 μm, which is about $0.07d$. The grid is stretched exponentially beyond $25d$ to form a buffer zone in which the maximum resolution increases to about $0.8d$. In the transverse y and z directions, the grid is stretched from the center to the boundaries. The resolution varies from about $0.026d$ to about $0.44d$. This places about 26 cells in the nozzle radius. The simulated near-field region of the jet, the jet exit Reynolds number, and the numerical resolution employed here are comparable with those in the LES studies of Uzun [49] and Anders [51].

The simulated pressure is 40 bar and the temperatures of the injected *n*-heptane vapor fuel and ambient gases are 1000 K. In the context of practical combustors, such as diesel engines, the choice of 1000 K for the air temperature is a realistic one, because the compression temperature in a diesel engine is typically about 1000 K [7]. However, note that injected fuel temperatures are generally lower ($\sim$400 K). Even though the near-stoichiometric regions in which the flame is located would have temperatures close to the air temperature (i.e., 1000 K) before combustion, regions close to the injector and near the jet centerline would have lower temperatures in a diesel jet. In the present case involving LES of a nonreacting jet, the choice of a higher fuel temperature (1000 K) leads to a lower injected-to-ambient gas density ratio of about 3.5, compared against a density ratio of about 8 with 400 K *n*-heptane temperature. However, it is expected that trends observed with respect to the computed turbulent statistics will be representative of diesel conditions, because density-ratio effects are known to show scaling behavior [52]. In the case of the flamelet calculations, the fuel temperature will influence chemical time scales, and we will comment on the implications of choosing a higher fuel temperature in Sec. IV.B.

For a jet diameter d of 1 mm, the jet exit Reynolds number of 70,000 corresponds to an injection velocity U_j of 42.5 m/s. This injection velocity is significantly lower than in modern diesel engines ($\sim$400 m/s), but the Reynolds number is comparable, due to the relatively large value of d. The ambient gas in the chamber consists of diluted air with 15% O_2 and 85% N_2, to simulate the presence of residual product gases in a diesel chamber. A relatively small coflow velocity U_{cf} of 0.425 m/s ($=0.01U_j$) is imparted to the ambient gas. The inclusion of U_{cf} is merely to decrease velocity gradients in the

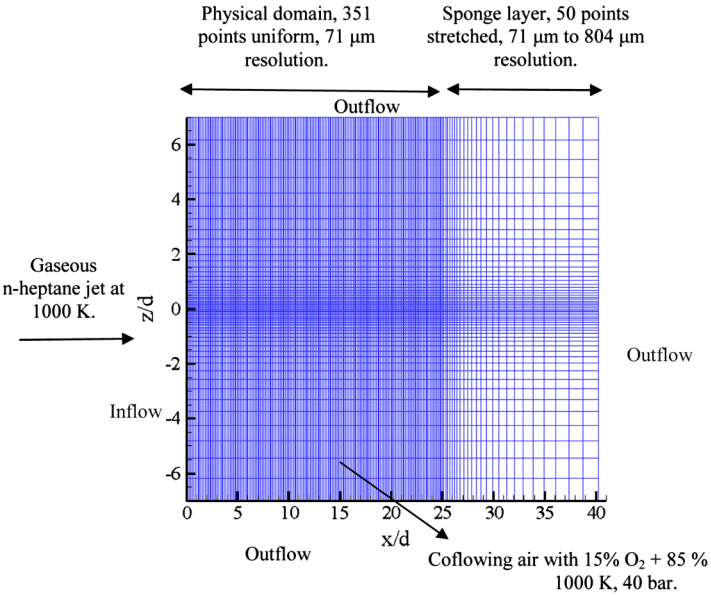

Fig. 2 The numerical grid employed in the LES studies, center z–x plane (every second grid point shown).

flowfield, and experimental data [53] indicate that for $U_{cf}/U_j <$ 0.08, the coflow velocity of the ambient fluid has negligible effects on the spreading characteristics of the jet. The maximum initial Mach number in the domain is about 0.15.

In this work, we are primarily interested in the statistically stationary jet structure. The flowfield is initialized with the steady self-similar solution of an incompressible turbulent round jet [50]. Then perturbations are introduced using the vortex-ring perturbation technique [23,25] close to the inlet ($x \sim 0.8d$) to trigger transition to an instantaneous turbulent flowfield corresponding to the conditions being simulated. Figure 3 shows the initial contours of filtered mixture fraction $\tilde{Z}$ in the simulated physical region of the jet, which is identical to the filtered fuel mass fraction for the nonreacting jet. Note that an initial shear-layer thickness θ about 30% of the orifice diameter d is employed [25]. Note in Fig. 2 that an initial guess of about $6d$ is used for the axial length of the potential core (i.e., the region of uniform $\tilde{Z}$), beyond which the self-similar profile [50] is imposed. Effects due to the initial potential core length, the initial self-similar profile, and the initial discontinuity in the transition region (see Fig. 2) disappear within one flow time ($=x_{\text{domain}}/U_j \sim 0.6$ ms) and have no bearing on the statistically stationary structure of the jet, which is of interest here.

The LES computation was performed in parallel with 128 3.2 GHz Intel Xeon processors. The simulation was performed for about 7 flow times, and temporal statistics were obtained over about 6 flow times to obtain converged statistics. Based on the approximately constant numerical time step ($\sim$1.6E − 8 s) and the CPU time per time step ($\sim$14 s), the CPU time for the computation was about 42 days.

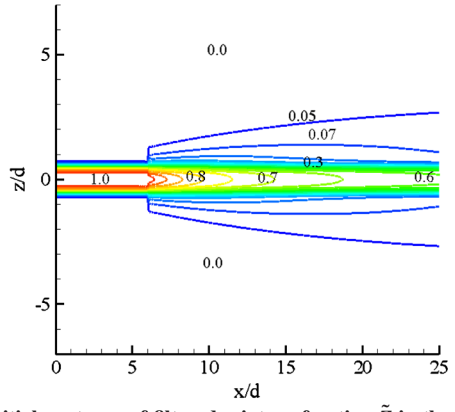

Fig. 3 Initial contours of filtered mixture fraction $\tilde{Z}$ in the center z–x plane of the jet.

B. Unsteady Flamelet Studies

To investigate the unsteady response of diffusion flamelets, the following unsteady flamelet equations [1,54] are solved:

$$\rho \frac{\partial Y_i}{\partial t} = \rho \frac{\chi}{2} \frac{\partial^2 Y_i}{\partial Z^2} + \dot{w}_i \tag{1}$$

$$\rho \frac{\partial h}{\partial t} = \rho \frac{\chi}{2} \frac{\partial^2 h}{\partial Z^2} - \sum_{i=1}^{N} h_i^0 \dot{w}_i \tag{2}$$

where Z is the mixture fraction; h is the mixture sensible enthalpy; ρ is the mixture mass density; Y_i, $\dot{w}_i$ and h_i^0 are the mass fraction, chemical production/destruction rate, and standard specific enthalpy of species i, respectively; and N is the total number of species. In Eqs. (1) and (2), χ is the instantaneous scalar dissipation rate, which is assumed to depend on Z according to the relation [1,54]

$$\chi = \frac{\chi_{\text{st}} \exp\{-2[\text{erfc}^{-1}(2Z)]^2\}}{\exp\{-2[\text{erfc}^{-1}(2Z_{\text{st}})]^2\}} \tag{3}$$

where χ_{st} is the instantaneous scalar dissipation rate at the stoichiometric mixture fraction Z_{st}. The functional form assumed in Eq. (3) is valid for both steady diffusion flames and unsteady mixing layers [1]. The stoichiometric scalar dissipation rate χ_{st} serves as an input parameter in the flamelet equations. Note that the flamelet equations considered here assume a unity Lewis number for all the species. Though we encounter a wide range of species Lewis numbers in n-heptane flames, the species with Lewis numbers significantly different from unity, such as H_2 and H, occur in relatively small proportions. For instance, our recent work on vortex-induced extinction/reignition of n-heptane flames [38] under pressures and temperatures similar to those considered in the present work show negligible differences in the flame temperatures and major species mass fractions between the unity Lewis number model and the mixture-averaged model for species transport. The governing equations are discretized in Z space using 102 grid points. The grid is significantly stretched about Z_{st} to achieve good resolution (about 12 grid points in a 10% thickness about Z_{st}) in the flame zone. Previous studies show that this grid is adequate to obtain grid-independent results [5]. Spatial discretization is achieved through second-order central differences and first-order backward temporal discretization is employed. Chemical kinetic source terms are computed through an

interface with CHEMKIN subroutines. The resulting discretized equations are solved using the Thomas algorithm. Note that this flamelet code has been employed in several previous studies of jet flames under diesel engine conditions [5,55,56].

In this work, we choose *n*-heptane as the fuel and describe its oxidation chemistry through a kinetic mechanism incorporating 159 species among 1540 reaction steps, developed by Seiser et al. [57]. Seiser et al. validated the 1540-step mechanism to predict autoignition delay times up to 100 bar and extinction strain rates at 1 bar. In addition, we have employed this mechanism in previous studies on autoignition [55] and extinction [5] under conditions similar to those employed here. Nevertheless, to the best of our knowledge, there is no experimental data on the structure and extinction of *n*-heptane diffusion flames (or even simpler fuels such as hydrogen and methane) at engine-relevant pressures (~40 bar). In the absence of experimental data for mechanism validation to predict extinction at high pressures, we will defer from drawing conclusions about reaction pathways and important chemical species for extinction/reignition in this work. However, we will characterize the flamelet characteristics through nondimensional numbers, such as the Damköhler number, so that the trends observed with respect to variation in the nondimensional parameters are expected to be valid with different kinetic mechanisms. The NO submechanism from GRI-Mech 3.0 is employed to describe NO formation.

In the section that follows, we will first present results of passive scalar statistics and turbulent time histories of χ computed using LES and then discuss the unsteady response of flamelets subjected to these time histories.

IV. Results and Discussion

A. LES: Passive Scalar Statistics and Scalar Dissipation Rate Time Histories

In this section, we will first present results of passive scalar (i.e., mixture-fraction statistics to validate the LES model employed here) and then discuss the generation of turbulent time histories of the scalar dissipation rate. Figures 4a and 4b show the instantaneous isocontours of the filtered mixture fraction $\tilde{Z}$ and the filtered scalar dissipation rate $\tilde{\chi}$ in the center z–x plane of the jet at 2.45 ms after the start of injection (ASI). Note from Fig. 4a that the stoichiometric isocontour $\tilde{Z} = 0.05$ appears to be significantly wrinkled and stretched. Moreover, the potential core region (i.e., region of uniform $\tilde{Z}$ in the axial direction) is observed to extend to about 8 jet diameters.

The filtered scalar dissipation rate $\tilde{\chi}$ shown in Fig. 4b is computed as [21]

$$\tilde{\chi} = 2(D_t + D_l)(\nabla\tilde{Z})^2 \tag{4}$$

where D_l is the laminar mass diffusivity and D_t is the turbulent mass diffusivity of the mixture, estimated as

$$D_t = \frac{\nu_t}{Sc_t} \tag{5}$$

In Eq. (5), ν_t is the eddy viscosity computed from the constant-coefficient Smagorinsky subgrid-scale model [25], and Sc_t is the turbulent Schmidt number, assumed to be 0.9 [25] in this work. We observe from Fig. 4b that relatively high values of $\tilde{\chi}$ (~500 s^{-1}) occur closer to the jet orifice ($x/d < 15$) and are interspersed by relatively low values, indicating strong spatial fluctuations. We will characterize the temporal fluctuations of $\tilde{\chi}$ later in this section. Now let us consider some of the mean temporal statistics of the mixture-fraction field and compare the computed values with available experimental data in self-similar jets.

The jet half-width $rz_{1/2}$ based on the mean mixture fraction $\bar{Z}$ is shown as a function of x/d in Fig. 5a. As expected, the jet spreads linearly, and the spreading rate, estimated as the slope of the linear fit to the computed data, is about 0.096. This value agrees within 15% with the measured range of 0.097–0.115 reported in experiments on variable-density jets of methane and propane with jet exit Reynolds numbers in the range of 4000–25000 [15,16,53] in the region $10 < x/d < 70$.

The reciprocal of the centerline mixture fraction, $1/\bar{Z}_{\mathrm{cl}}$, is shown in Fig. 5b as a function of x/d_e, where d_e is an effective jet diameter accounting for density-ratio effects [43], given by

$$d_e = d \cdot (\rho_j/\rho_a)^{1/2} \tag{6}$$

In Eq. (5), d is the jet diameter, and ρ_j and ρ_a are the injected and ambient gas densities, respectively. In the present case, ρ_j/ρ_a is about 3.5, and hence $d_e \sim 1.86d$. A decay rate of 0.192 is estimated from the linear fit to the computed data, which is reasonably close (within 25%) to the range of 0.212–0.25 reported in the measurements [15,16,53]. Note that apart from the inadequacies of the constant-coefficient Smagorinsky model employed here, the observed discrepancies may be related to the lack of self-similarity in the simulated near field ($x/d < 30$) of the jet.

To explore the self-similarity of the computed mean mixture-fraction field in the jet near field, consider Figs. 6a and 6b, which show the radial profiles of the normalized mean mixture fraction $\bar{Z}/\bar{Z}_{\mathrm{cl}}$ and the square root of the normalized filtered variance $(\bar{Z}''^2/(\bar{Z}''^2)_{\mathrm{cl}})^{1/2}$, respectively. Computed and measured results are shown. We observe from Fig. 6a that even though the mean mixture-fraction field lacks self-similarity in that the profiles at different axial locations are not superimposed, the computed values agree well (within 10%) with measurements. Similarly, the variance field clearly lacks self-similarity in the simulated jet near field, as seen from Fig. 6b, but the peak values and locations of the peaks are reasonably close (within 20%) to the measured values in the region, $0 < r/rz_{1/2} < 2$. Now we will characterize the means and fluctuations of the scalar dissipation rates in the jet.

Figure 7 shows the computed radial profiles of the time-averaged conditional-mean scalar dissipation rate $\tilde{\chi}_Z$ at different axial

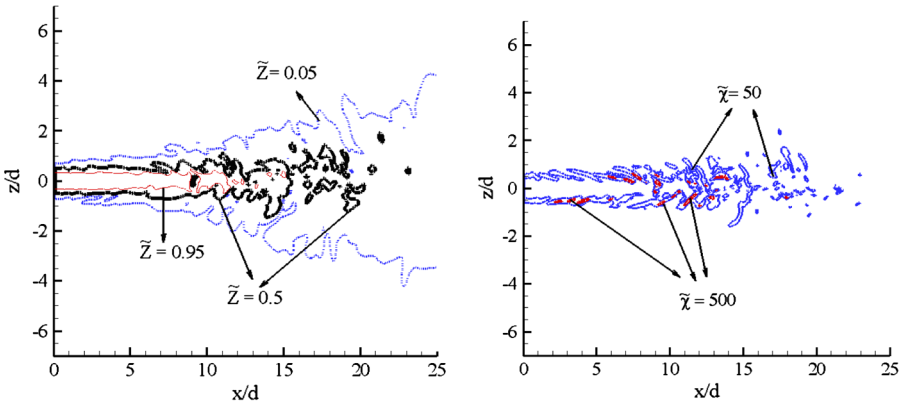

Fig. 4 Instantaneous isocontours in the center z–x plane of a) filtered mixture fraction $\tilde{Z}$ and b) filtered scalar dissipation rate $\tilde{\chi}$ at 2.45 ms ASI.

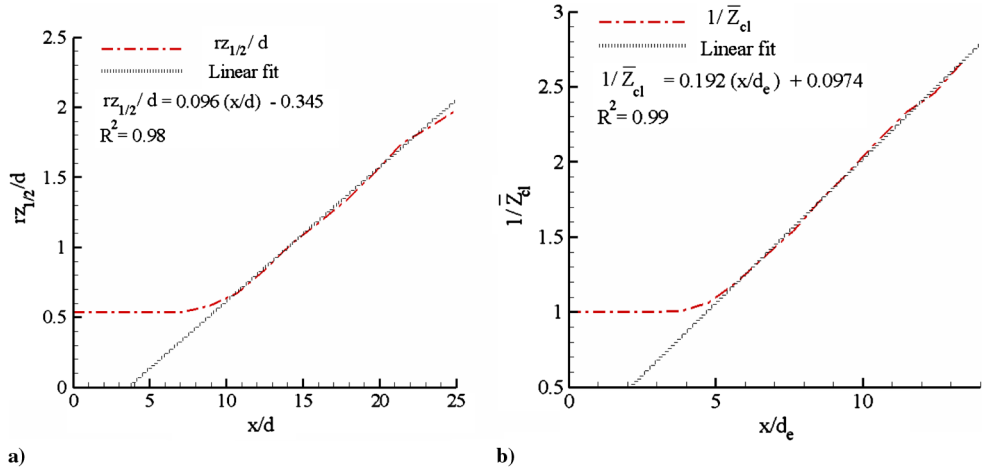

Fig. 5 Mean jet spreading rate in terms of a) mixture-fraction half-width $rz_{1/2}$ and b) inverse of centerline mixture fraction ($1/\bar{Z}_{cl}$).

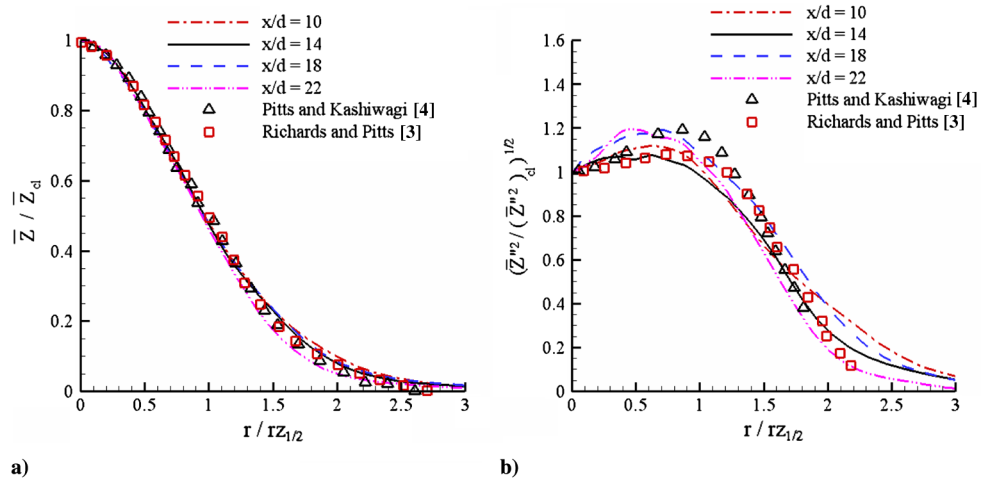

Fig. 6 Computed radial profiles of a) normalized mean mixture fraction $\bar{Z}/\bar{Z}_{cl}$ and b) square-root of normalized filtered variance $(\bar{Z}''^2/(\bar{Z}''^2)_{cl})^{1/2}$ in the jet.

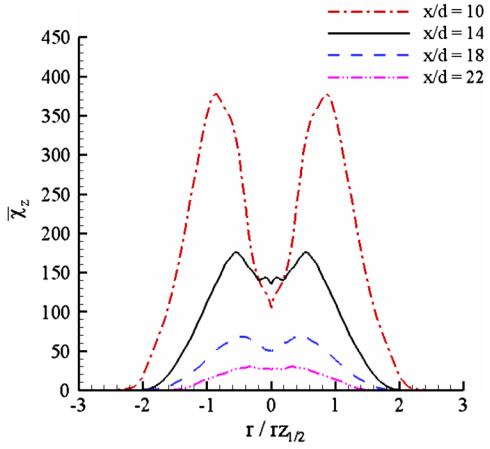

Fig. 7 Computed radial profiles of time-averaged conditional-mean scalar dissipation rate $\bar{\chi}_Z$ in the jet.

locations in the jet. Following Bushe and Steiner [58], the conditional-mean scalar dissipation rate χ_Z is related to the filtered value $\tilde{\chi}$ by the expression

$$\tilde{\chi} = \int_{Z=0}^{Z=1} \chi_Z P_Z(Z, \bar{Z}, \bar{Z}''^2)\mathrm{d}Z \tag{7}$$

where P_Z is the subgrid-scale probability density function (PDF) of the mixture fraction, which is, in general, a function of $\bar{Z}$ and $\bar{Z}''^2$. In the present work, we assume that P_Z is a beta PDF, shown to be a good estimate for the subgrid-scale PDF of the mixture fraction in reacting DNS studies of homogenous turbulence [59], and widely employed in LES studies of reacting jets [12,34]. Moreover, the functional dependence of χ_Z on Z is presumed according to Eq. (3) [1,58], and so χ_Z and the conditional-mean scalar dissipation rate χ_{st} conditioned on the stoichiometric mixture fraction are given by the expressions

$$\chi_Z = \chi_{st} f(Z) \tag{8}$$

and

$$\chi_{st} = \frac{\tilde{\chi}}{\int_{Z=0}^{Z=1} f(Z) P_Z(Z, \bar{Z}, \bar{Z}''^2)\mathrm{d}Z} \tag{9}$$

In Eqs. (8) and (9), $f(Z)$ is the inverse complementary error function profile given in Eq. (3). Note that in using Eq. (3), we assume that the functional dependence of χ_Z on Z is not bimodal. From the LES data, this lack of bimodality was found to be true in the case of the filtered value $\tilde{\chi}$ as well. We observe from Fig. 7 that $\bar{\chi}_Z$ shows the characteristic double-peak profile reported in measurements [17]. Moreover, consistent with measured trends [17,18], $\bar{\chi}_Z$ strongly decays ($\sim x^{-4}$) as we proceed downstream in the jet due to turbulent mixing.

The time evolution of the scalar dissipation ratio [33,38], χ_r, is shown in Fig. 8 at the jet location $x/d = 12$ on the jet centerline, where χ_r is computed as

$$\chi_r = \frac{\chi_{st}}{\chi_e} \tag{10}$$

In Eq. (9), χ_e is the steady extinction limit, equal to 500 s^{-1} for the simulated pressures and temperatures (to be discussed in Sec. IV.B). We observe strong temporal fluctuations of χ_r in Fig. 8. It is interesting to note that large values of χ_r ($\sim$1) are relatively short-lived and are often followed by relatively small values (less than 0.1). Consequently, the mean value at the chosen jet location (i.e., $x/d =$ 12 and $r/d = 0$) is relatively small ($0.04\chi_e$). We will now characterize the temporal PDF of χ_{st} at different locations in the jet.

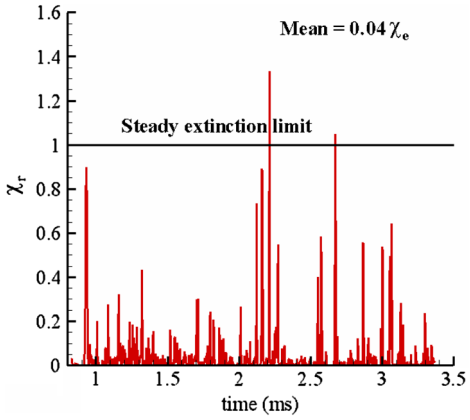

Fig. 8 Time evolution of χ_r at the jet location $x/d = 12$ and $r/d = 0$.

Figures 9a–9d show the computed PDFs of $\ell_n(\chi_{st})$ at different locations in the jet. Also shown in the figures is a normal distribution, computed as

$$P_N(\ell_n(\tilde{\chi})) = \frac{1}{\sqrt{2\pi}\sigma}\exp\left(-\frac{(\ell_n(\tilde{\chi}) - \mu)^2}{2\sigma^2}\right) \tag{11}$$

where μ and σ represent the mean and root-mean-square (rms) values of $\ell_n(\tilde{\chi})$, respectively, computed from the turbulent time records at different locations in the jet. Note that data collected over 100,000 time steps were used for the evaluation of the PDF. Figures 9a–9d show that the normal distribution describes the PDF of $\ell_n(\chi_{st})$ reasonably well, particularly at downstream jet locations (see the results for $x/d = 16$). In other words, consistent with the experimental findings of Effelsberg and Peters [18], the lognormal distribution is a reasonable approximation for the PDF of the scalar dissipation rate. Reacting LES studies [53] have also reported good agreement of the scalar dissipation rate PDF with the lognormal distribution. Figures 9a–9d show that the discrepancies between the lognormal distribution and the computed PDFs arise primarily at the tails (i.e., at relatively high and relatively low values of the scalar dissipation rate). Interestingly, these represent low-probability events that are expected to be important for extinction/reignition and may not be captured by a universal distribution, such as the lognormal distribution. These events may be specific to the simulated jet.

The reasonable agreement of the computed results with measurements in terms of both qualitative and quantitative trends discussed so far lends credence to the computed results. Now we will discuss the generation of χ_{st} time histories, which can be employed to investigate the unsteady response of flamelets. Note that the turbulent

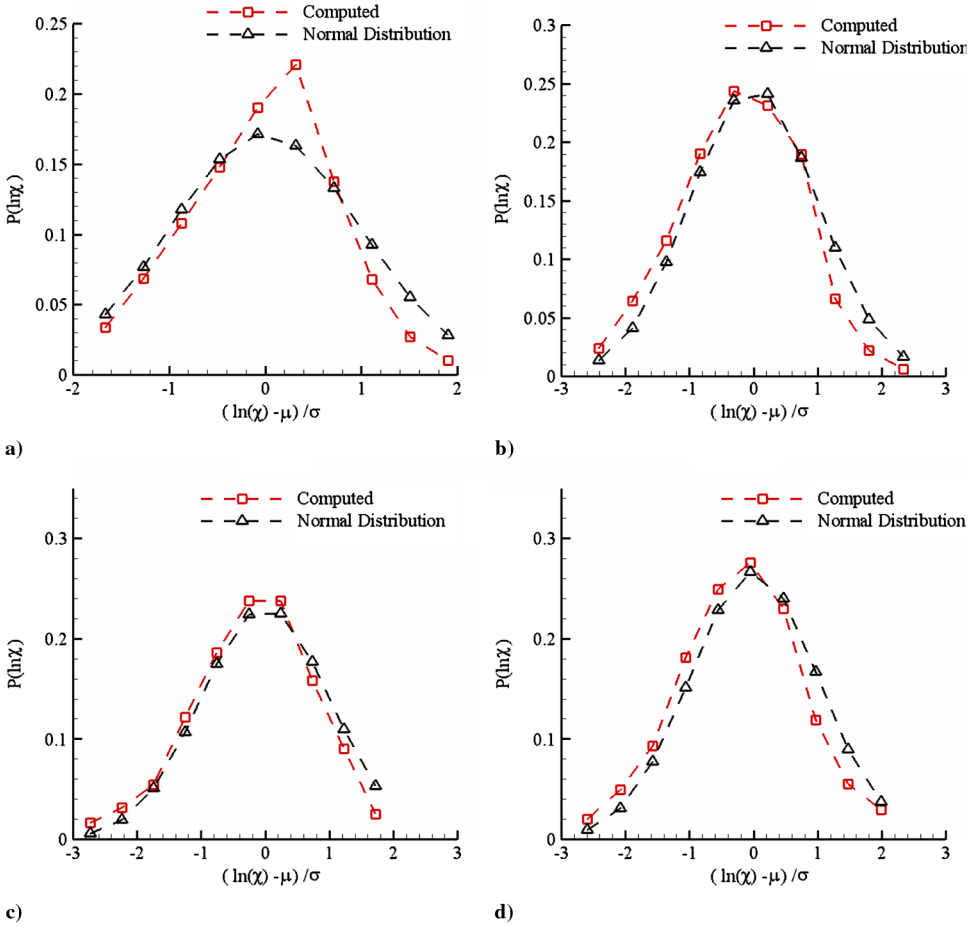

Fig. 9 Comparison of the computed temporal PDF of χ_{st} with a lognormal distribution at a) $x/d = 12$ and $r/d = 0$, b) $x/d = 16$ and $r/d = 0$, c) $x/d = 12$ and $r/d = 0.5$, and d) $x/d = 16$ and $r/d = 0.5$.

time record shown in Fig. 8 at the jet location $x/d = 12$ may be viewed as fluctuations due to the passage of multiple eddies through that location. In a reacting jet, these eddies will correspond to a flamelet. In other words, to generate turbulent time histories of the scalar dissipation rates experienced by the flamelets in the near field of the jet, we need to employ Lagrangian-type tracking of stoichiometric isocontours in space and time. Tracking *stoichiometric* contours is consistent with the flamelet concept that assumes flamelets to be very thin regions about the stoichiometric mixture fraction [1]. The tracking procedure and results are discussed next.

To track a flamelet originating from a given axial location, the following algorithm is employed. At a given time instant, the stoichiometric mixture-fraction isocontour is computed as

$$r_f^n = f^n(x_f^n) \tag{12}$$

where r_f^n and x_f^n represent the radial and axial locations of the flamelet at the nth time level, respectively. Moreover, the instantaneous scalar dissipation rate χ_{st}^n at a given time level and axial location is estimated as

$$\chi_{st}^n = \chi_{st}|_{x_f^n, r_f^n} \tag{13}$$

where $\chi_{st}|_{x_f^n, r_f^n}$ is the conditional-mean scalar dissipation rate conditioned on the stoichiometric mixture fraction, computed using Eq. (9) at the location (x_f^n, r_f^n). As discussed by Peters [1], the conditional-mean χ_{st} accounts for subgrid fluctuations (through a presumed subgrid PDF of the mixture fraction) and, hence, is an appropriate parameter in the flamelet equations. The radial location r_f^n is computed as a number average of all radial distances, where $\tilde{Z} = Z_{st} \pm 0.05Z_{st}$ at a given axial location x_f^n. At the next time level, the x displacement of the flamelet is computed as

$$x_f^{n+1} = x_f^n + \tilde{u}_f^n \Delta t - \frac{\nabla \cdot (\rho D \nabla Z)}{\rho |\nabla Z|^2} \frac{\partial Z}{\partial x} \Delta t \tag{14}$$

where $\tilde{u}_f^n$ is the instantaneous axial velocity at the stoichiometric mixture fraction at a given axial location (computed as a number average over $\tilde{Z} = Z_{st} \pm 0.05Z_{st}$ similar to r_f^n). In Eq. (14), the third term on the right-hand side represents the axial component of the diffusive velocity of the mixture fraction [34]. Because mixture-fraction gradients are stronger in the radial direction, the axial contribution of the diffusive velocity of the mixture fraction is expected to be negligible [34]. Furthermore, in the present case, the axial convection velocities are relatively large in the jet near field and would outweigh the axial diffusive velocities. Hence, the flamelet trajectories are computed using the convection velocities alone in Eq. (14). Once x_f^{n+1} is known, r_f^{n+1} can be computed knowing the stoichiometric contour at the $n + 1$ time level as

$$r_f^{n+1} = f^{n+1}(x_f^{n+1}) \tag{15}$$

In addition, χ_{st}^{n+1} can be estimated using Eq. (13) for the $n + 1$ time level. Flamelets that originate at different axial locations in the jet (i.e., with different x_f^0) will be subject to different χ_{st} time histories as they traverse through the jet.

In the present case, we generate 10 representative scalar dissipation rate χ_{st} time records spanning a time interval of 3.5 ms (about 6 flow times in the jet) and the region $6 < x/d < 20$. Henceforth, we will refer to these time records as flamelet histories to indicate that these time records are employed to investigate the unsteady response of flamelets. The 10 representative flamelet histories originate from different axial locations in the jet. In particular, flamelets 1–10 are tracked in time and space using the stoichiometric isocontours originating from $x/d = 6, 6.25, 6.5, 7.0, 7.25, 8.0, 8.5, 9.5, 10.5$, and 11.0 in the jet, respectively. For instance, consider Fig. 10, which shows the computed paths of three flamelets originating at $x/d = 6$ (flamelet 1), 7.25 (flamelet 5), and 11 (flamelet 10). Figure 11 shows the three corresponding χ_{st} time histories. The differences in the time histories illustrate the unsteady and intermittent nature of the turbulent jet. We observe that whereas the flamelet originating at an upstream jet location (i.e., flamelet 1) is subjected to a relatively large number of peaks in χ_{st}, the downstream flamelets predominantly encounter relatively low values. Recall from our earlier discussion that we observed similar trends in the time-averaged conditional-mean scalar dissipation rates $\tilde{\chi}_Z$ in the jet near field, which were found to decrease with axial location in the jet. Note that the time records have been obtained from the unsteady LES data collected every 0.01 ms. Hence, it is possible that some of the additional peaks of χ_{st} (for instance, see Fig. 8) have not been captured in the records. However, such peaks would also be short-lived and may not significantly influence the flame response.

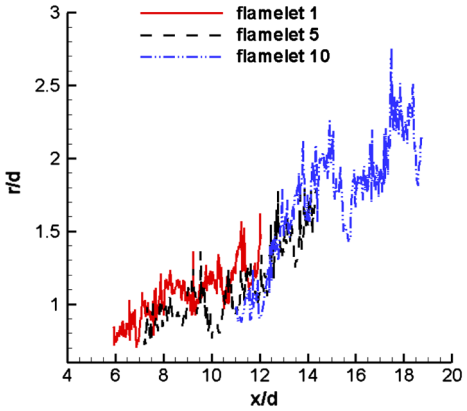

Fig. 10 Paths of three flamelets originating at different axial locations in the LES jet flowfield.

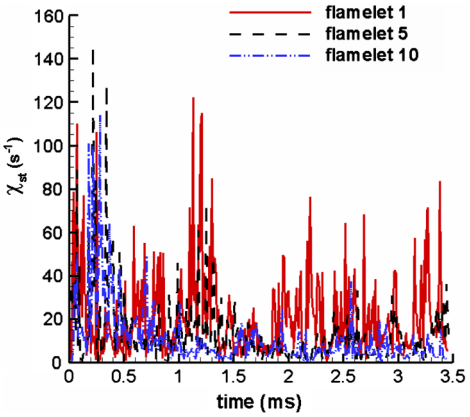

Fig. 11 Time histories of χ_{st} (s^{-1}) for three flamelets originating at different axial locations in the LES jet flowfield.

In the following section, we will first quantify the steady extinction characteristics and then investigate the unsteady flame response to fluctuations of the scalar dissipation rate. In the subsequent analysis, we choose the stoichiometric mixture fraction Z_{st} as the diagnostic point.

B. Unsteady Flamelet Studies

Before we characterize unsteady flame response, it is useful to quantify the steady behavior of the flamelets investigated in this work. Figure 12 shows the temperature T_{st} and chemical heat release rate Q_{st} at Z_{st} as a function of χ_{st}. As expected, T_{st} decreases as χ_{st} increases, due to the diffusive loss of heat and radicals to richer and leaner fractions. Note that Q_{st} increases initially, up to about $\chi_{st} = 75\ s^{-1}$, as a result of enhanced mixing, but decreases thereafter due to the opposing effect of decreasing flame temperatures. These trends are in agreement with asymptotic theory [60]. In addition, note that due to relatively shallow temperature gradients close to extinction, the flame becomes increasingly insensitive to large values of χ_{st} (greater than 300 s^{-1}). It is interesting that for the chosen conditions (i.e., a pressure of 40 bar and fuel and oxidizer

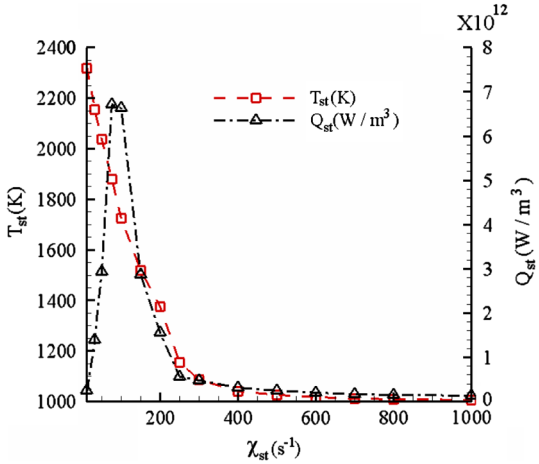

Fig. 12 T_{st} (K) and Q_{st} (W/m^3) as a function of χ_{st} (s^{-1}) from steady flamelet solutions.

temperatures of 1000 K), we obtain a stretched S curve [61], as seen from Fig. 12. In other words, there is no distinction between steady ignition and steady extinction limits in the present case, and so the steady extinction limit χ_e serves as a useful parameter to characterize the chemical time scale of the flame.

In this work, we define the extinction point as the value of χ_{st} at which the frozen solution ($T_{st} = T_a = 1000$ K, where T_a is the air-side temperature) is reached. From Fig. 12, at $\chi_{st} = 500$ s^{-1}, T_{st} is within 3% of 1000 K, and the maximum temperature (at $Z \sim 0.3$) was found to be within 8% of T_a. Here, we will assume that this condition to be close enough to the frozen solution and hence choose $\chi_e = 500$ s^{-1}. It is realized that this is somewhat arbitrary, and one may choose even higher values to reach closer to frozen flow. Furthermore, alternative criteria for the determination of χ_e can also be employed: for instance, the turning point of Q_{st} [32], which corresponds to $\chi_{st} = 75$ s^{-1} in Fig. 12. In the present case with $T_{fuel} = T_a = 1000$ K, these two criteria yield significantly different values. This will change the range of Damköhler numbers based on χ_e (to be discussed), but not the underlying physical mechanisms governing unsteady flame response. Now we will investigate the unsteady response of flames subjected to oscillatory perturbations.

It is useful to characterize the generated histories in terms of a mean and root-mean-square (rms) value, which also determine the temporal PDF. Figure 13 shows the computed mean and rms of the 10 flamelet histories. It is interesting to note that the mean values are relatively small (less than $0.06\chi_e$), because the relatively large values of χ_{st} are short-lived in all the cases. We observe from Fig. 13 that the rms and the mean values show similar trends. Note that whereas increasing the mean values would increase the peaks that may lead to flame extinction/flame weakening, increasing the rms values would decrease the minimum values of χ_{st} (in addition to increasing the peaks) that may favor reignition and/or flame recovery. Based on the

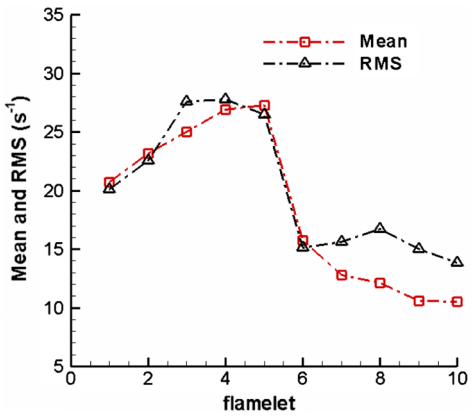

Fig. 13 Means and rms values of the generated flamelet histories.

mean value of χ_{st} for a flamelet history, $\langle\chi_{st}\rangle$, which represents the inverse of a mean mixing time scale, and the steady extinction limit χ_e, which represents the inverse of a characteristic chemical time scale [9], we can define a Damköhler number Da as

$$Da = \frac{\chi_e}{\langle\chi_{st}\rangle} \tag{16}$$

Note that $\langle\chi_{st}\rangle$ is distinct from $\bar{\chi}_{st}$, which represents the temporal mean of χ_{st} at a given axial location. In other words, $\langle\chi_{st}\rangle$ represents the mean value of χ_{st} experienced by a flamelet as it traverses through time and space in the simulated near field of the jet. Hence, the values of Da corresponding to the range of values of $\langle\chi_{st}\rangle$ shown in Fig. 13 would represent the range of Damköhler numbers of flamelets that are likely to be encountered in the jet near field. These Da values lie in the range of 15–50, which represent moderately strained flamelets reasonably far from extinction. We will also consider highly strained flamelets ($Da \sim 1$) in the subsequent analysis to clarify the effects of Da on the unsteady flame response. Let us now consider the unsteady responses of the flame temperature and species to fluctuations of χ_{st}.

Figures 14a–14c show the responses of T_{st} and the mass fractions of CO_2 and H_2O as a function of χ_r for flamelet history 3, respectively. Note from Fig. 13 that flamelet history 3 has the maximum values of mean ($\sim 0.06\chi e$) and variance ($\sim 0.06\chi e$) of the 10 flamelets considered. In Figs. 14a–14c, predictions using a steady flamelet library are shown for comparison. The steady flamelet library was constructed using steady solutions corresponding to 21 values of χ_{st} in the range of $(0.002–4.0)\chi_e$. Interpolation based on each value of χ_{st} from the turbulent time record is then employed to obtain the temperature and species response corresponding to the steady flamelet. Note that for the unsteady cases, the initial condition is the steady flamelet solution corresponding to the initial value of χ_{st} in the time record.

The unsteady temperature response to flamelet history 3 involves temporary flame-weakening events at relatively large values of χ_r (greater than 0.3), followed by flame recovery at relatively small values of χ_r. We observe from Fig. 14a that the trends in T_{st} values predicted by both unsteady and steady flamelet calculations agree reasonably well. However, the steady flamelet model does not describe the transient flame weakening and recovery well. For instance, T_{st} at the maximum value of χ_r (~ 0.6) at about 1.93 ms is underestimated by about 38% by the steady flamelet model in comparison with the unsteady flamelet model. Such discrepancies can have important implications for relatively sensitive species such as NO. Let us now consider the unsteady response of the major species CO_2 and H_2O and the pollutants NO and unburned hydrocarbon (UHC).

Figures 14b and 14c compare steady and unsteady flamelet predictions for the mass fractions of CO_2 and H_2O, respectively. Comparing Figs. 14a and 14b, we observe good qualitative agreement in the unsteady responses of T_{st} and CO_2. In comparison with CO_2 response, Fig. 14c shows relatively good agreement between steady and unsteady flamelet predictions for H_2O, indicating faster chemical-response time scales. To quantify this observation, we can estimate characteristic chemical time scales τ_{ck} for the species as

$$\tau_{ck}^{-1} = \frac{|\dot{w}_{ck}| \cdot \mathrm{MW}_{mix}}{\rho} \tag{17}$$

where $\dot{w}_{ck}$ is the net molar chemical production rate of species k, MW_{mix} is the mixture molecular weight, and ρ is the mixture density. Note that the definition in Eq. (17) is similar to the chemical time scale defined in the flame–vortex simulations of Safta et al. [62] with a single-step kinetic model. For instance, at $\chi_{st} = 0.1\chi_e$, $\tau_{ck,CO_2} = 0.16$ ms, whereas $\tau_{ck,H_2O} = 0.02$ ms. Hence, consistent with the ordering of the chemical time scales, H_2O shows a faster response and recovery during reignition in comparison with CO_2. Also, $\tau_{ck,NO} = 6.41$ ms and $\tau_{ck,UHC} = 0.19$ ms, implying that UHC is expected to respond much faster to χ_{st} fluctuations relative to NO.

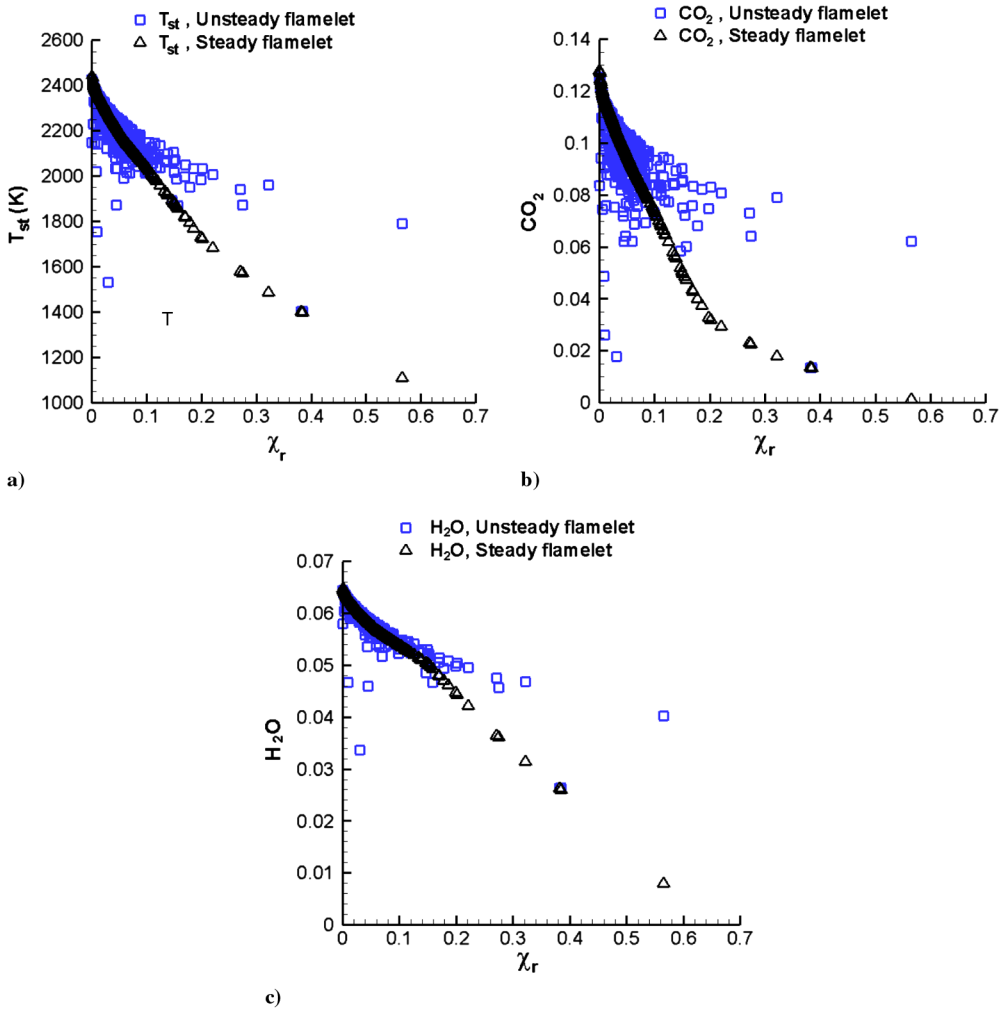

Fig. 14 Response of a) T_{st} (K), b) CO_2 mass fraction, and (c) H_2O mass fraction as a function of χ_r for flamelet history 3 with unsteady and steady flamelets.

Figures 15a and 15b show the responses of NO and UHC to flamelet history 3. NO response shows significant differences between steady and unsteady flamelet predictions. Note that in the case of flamelet history 3, we begin with a relatively large value of χ_r (∼0.38), and hence the initial NO mass fraction is negligibly small due to the associated low temperatures (∼1400 K). Following the rapid decrease in χ_r, the steady flamelet model predicts an immediate increase in NO mass fraction, whereas the unsteady flamelet calculation predicts a delayed response due to the relatively slow response times of NO. Consequently, the steady flamelet model overestimates peak values during the unsteady response by as much as 1.5–2 times in comparison with the unsteady flamelet calculations. Hence, even for the relatively small excursions of χ_{st} above χ_e (i.e., $\chi_r < 1.0$) considered here, steady flamelet models are inadequate to predict transient NO response. On the other hand, UHC shows much faster response to χ_{st} fluctuations, as seen from Fig. 15b. The steady flamelet model significantly overestimates UHC values at larger values of χ_r (greater than 0.3), but due to fast response times, the UHC mass fractions relax to values closer to steady values at the lower values of χ_r. Moreover, note that in the present case, the

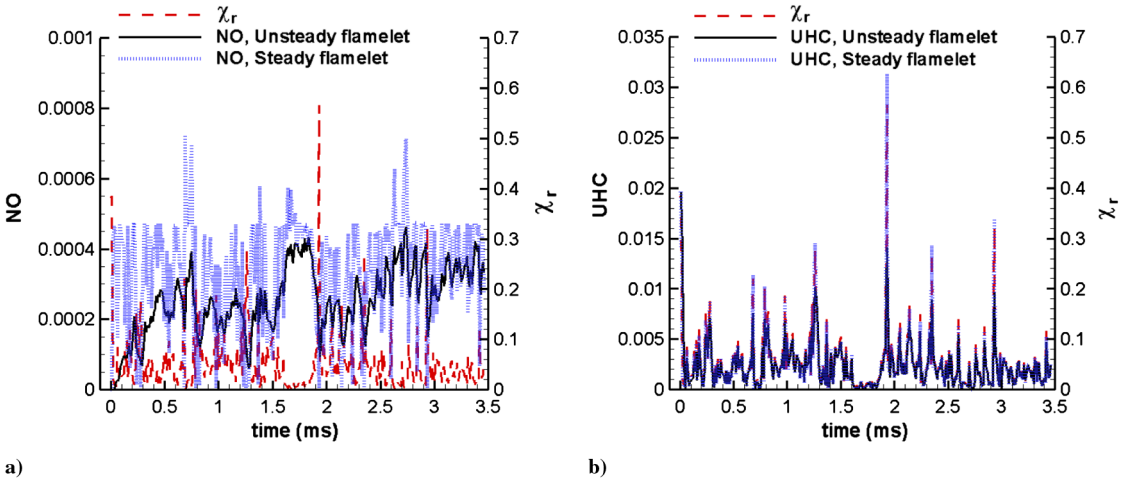

Fig. 15 Unsteady response of a) NO and b) UHC to flamelet history 3 using unsteady and steady flamelet models.

majority of the values of UHC mass fraction are relatively low (less than 0.005), due to the absence of extinction and the associated high temperatures.

It is useful from a modeling perspective to compute the (temporal) mean temperature at different axial locations from the flamelet histories and to compare the predictions from unsteady and steady flamelet models. Figures 16a and 16b show the mean T_{st} and NO mass-fraction values computed from the flamelet histories using unsteady and steady flamelet calculations. In other words, the mean T_{st} at each axial location is computed as an average over all the flamelets passing through that location. Because different flamelets pass through a given axial location at different instants of time, the mean values shown in Figs. 16a and 16b represent temporal means. We observe from Fig. 16a that the agreement between the models with respect to mean T_{st} is within 5%. Hence, the relatively small differences between the two models even at upstream jet locations confirm the low probability of events with relatively large values of χ_{st}, which do not significantly affect the mean. Note that because all the tracked flamelets do not penetrate to the downstream jet locations ($x/d = 17$ and 18, for instance) during the duration of 3.5 ms, the number of flamelet histories over which averaging is performed decreases at these locations. However, because we predominantly encounter lower values and lower-intensity fluctuations of χ_{st} at downstream regions, the estimates of the mean temperatures and major species mass fractions are reasonable. Though not shown here, mean UHC predictions with the steady flamelet model agreed well with unsteady flamelets.

Note from Fig. 16b that the differences are greater (up to 20% at $x/d = 12$) with respect to NO due to its relatively high temperature sensitivity and phase-lag effects, but the predictions from both the models agree reasonably well. Hence, in the present case, steady flamelet models are adequate for the prediction of mean temperature, major species, and UHCs and are reasonable for the prediction of the mean concentration of pollutants such as NO. This is a useful result from a modeling perspective, because steady flamelets are easier to implement as a reacting LES submodel compared with unsteady flamelets and do not require the use of an additional tracking scalar, such as the progress variable [63], to capture the time coordinate and are therefore computationally more efficient.

In the results presented so far, we did not account for radiative heat losses from the flame zone. The review of flamelet structure and extinction by Williams [60] shows that radiant energy losses become significant only under very low strain rates (i.e., far from strain-induced extinction), and the presence of shallow gradients and high-temperature zones result in relatively high rates of radiative losses. In *n*-heptane flames, such losses would primarily result from soot radiation. Hence, it is expected that when the flamelets experience low strain rates in the fluctuating time record, radiative losses may act to further increase the chemical-response times. This would further increase the discrepancies between steady and unsteady flamelet models, particularly for sensitive species, such as NO.

In addition, although the results discussed so far are useful to understand unsteady flame response in turbulent flowfields and the applicability of steady flamelet models, the predicted temperatures and species mass fractions and their axial variations (for instance, Figs. 16a and 16b) are likely to differ in a reacting LES computation. In the present case, the χ_{st} time histories are generated from a nonreacting jet flowfield and do not include the feedback effects due to combustion heat release. In addition, the flamelet histories generated here correspond to the unsteady near field of a 70,000-Reynolds-number jet. In practical combustors, such as diesel engines, although the injection velocity U_{inj} employed may be more than an order of magnitude higher than that employed here, the orifice diameters d may be order of magnitude smaller. This implies that though the chosen jet Reynolds number of 70,000 may be representative of diesel engine applications, the global strain rates U_{inj}/d would be 1 to 2 orders of magnitude higher for diesel jets. Hence, it is useful from a practical perspective to extrapolate the present analysis to a higher-strain-rate jet, in which stronger fluctuations of χ would be encountered. In the section that follows, we consider stronger scalar dissipation rate fluctuations and investigate the potential impact of unsteady extinction/reignition events on the unsteady flame response, applicability of steady flamelets, and jet near-field phenomena such as flame liftoff. In addition, fuel temperatures are typically lower (~400 K) in diesel engine applications than those employed here (1000 K), which can result in relatively weaker (or strained) flamelets ($Da \sim 1$). Hence, we will also explore the possible implications of employing a lower fuel temperature in the following sections.

1. *Extrapolation to a Higher-Strain-Rate Jet*

In the present case, we consider a moderate increase by a factor of 5 to demonstrate the influence of stronger fluctuations of the scalar dissipation rate on the unsteady flame response. Under the assumption that the cumulative distribution function (CDF) of the fluctuating time records of χ_r computed from the present LES jet remains valid for a higher-strain-rate jet, we can generate flamelet histories with higher means and rms values. In other words, if the CDF remains constant, the following expression can be used:

$$\frac{\chi_{r1} - \mu_1}{\sigma_1} = \frac{\chi_{r2} - \mu_2}{\sigma_2} \tag{18}$$

where subscripts 1 and 2 refer to the lower- and higher-Reynolds-number cases, respectively, and μ and σ represent the mean and the rms, respectively. Here, we consider $\mu_2 = 5\mu_1$, and $\sigma_2 = 5\sigma_1$ to generate the fluctuating time records. It is clear from Fig. 11 that with higher means and rms values, there are repeated excursions of χ_r above unity (i.e., $\chi_{st} > \chi_e$). Note that when the means are increased 5 times, the maximum value of the mean among the 10 flamelet histories considered is about $0.3\chi_e$. Let us now explore the unsteady

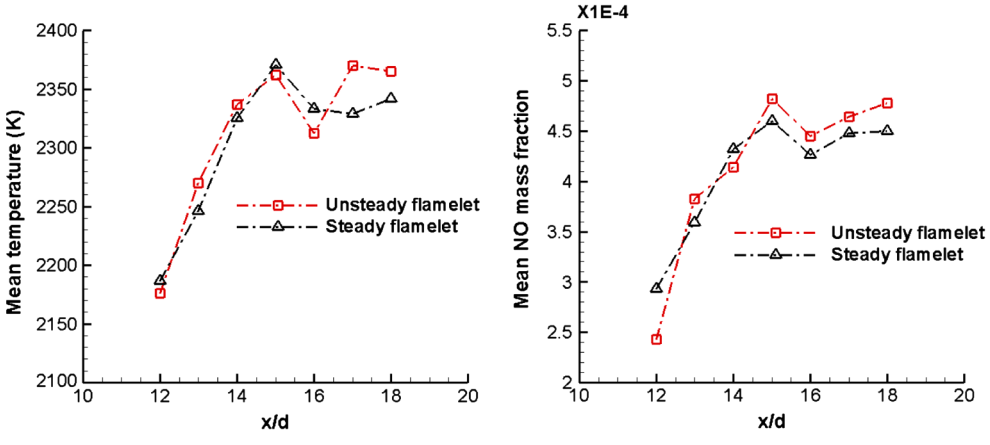

Fig. 16 Mean values of a) T_{st} (K) and b) NO mass fraction computed from the flamelet histories as a function of axial location in the jet.

temperature and species responses for the flamelet histories with higher means and variances.

Figures 17a–17c show T_{st} and the mass fractions of NO and UHC as a function of χ_r, respectively, for flamelet history 3 when μ and σ are increased 5 times. In this case, the unsteady flame approaches local extinction, indicated by the relatively low temperatures (less than 1400 K) at the larger values of χ_r(>1.0), as seen from Fig. 17a. Moreover, in qualitative agreement with previous studies in the literature focusing on oscillatory[26–30] and vortex-induced [32,33] perturbations, the unsteady flame is more resistant to extinction, due to chemical phase-lag effects, and does not reach frozen flow (i.e., $T \sim 1000$ K) even at the maximum χ_r value of about 3. Moreover, Fig. 17a shows that the transient reignition involves partially burned states that cannot be represented uniquely by a parameterization solely in terms of χ_{st}: that is, $T_{st} = fn(\chi_{st})$, where fn is the functional relationship derived from the steady flamelet equations [i.e., Eqs. (1) and (2) without the unsteady term]. A reactive scalar, such as the reaction progress variable [1,63] c_{st}, has to be used to distinguish the transient states during reignition from those during extinction. Hence, from a turbulent combustion-modeling viewpoint, an unsteady flamelet/progress variable model [64] is more appropriate than steady flamelets to simulate the transient extinction/reignition phenomena observed here. As in the recent works of Pierce and Moin [63] and Pitsch and Ihme [64], the progress variable c can be modeled as the sum of major species mass fractions, and the mean/filtered value can be solved through a transport equation in a RANS/LES submodel. Furthermore, note from Figs. 14a and 17a that we observe much greater deviations between the steady and unsteady flamelet predictions as the mean and rms of χ_{st} fluctuations increase. Conceptually, these trends are similar to those in oscillatory [26–30] and vortex-induced [32,33] perturbation studies, which indicate increasing departures from steady behavior with increasing χ_{st} amplitudes and frequencies or increasing vortex velocity scales. We will now investigate the response of species to the turbulent time records with higher means and rms values. The major species (e.g., CO_2) show trends similar to those in the temperature, and hence we will only discuss, for brevity, the responses of NO and UHC.

Figures 17b and 17c show the unsteady responses of NO and UHC mass fractions, respectively, to the flamelet history 3 with higher μ and σ. Figure 17b shows that NO formation is significantly suppressed due to local extinction events, which occur with a higher probability in this case. Furthermore, due to relatively slow chemical-response times, NO fails to recover even during the reignition events in spite of the associated relatively high temperatures (greater than 2200 K). Hence, these trends indicate that unsteady extinction/reignition events are beneficial both in terms of flame stability, because they prevent complete extinction of the flame, and NO formation control. Note that as μ and σ increase, not only do the χ_{st} amplitudes increase, these amplitudes also occur with a higher frequency (or probability). In other words, with higher mean and rms values, we encounter shorter mixing times (i.e., higher amplitudes) and shorter residence times (i.e., higher frequencies), which have significant effects on slower species such as NO. The experiments of Barlow and Frank [35] in Sandia flames A–F indicate significant suppression of NO formation as one proceeds from flame A to flame F with increasing Reynolds numbers and increasing levels of local extinction/reignition. The authors suggest decreasing residence times as a possible explanation for NO suppression. Furthermore, the strong dependence of NO formation on residence times has been reported in engines as well [65]. As expected, the steady flamelet model grossly overestimates NO mass fractions at several instants, due to its inherent inability to account for transient extinction/reignition and the associated phase-lag effects.

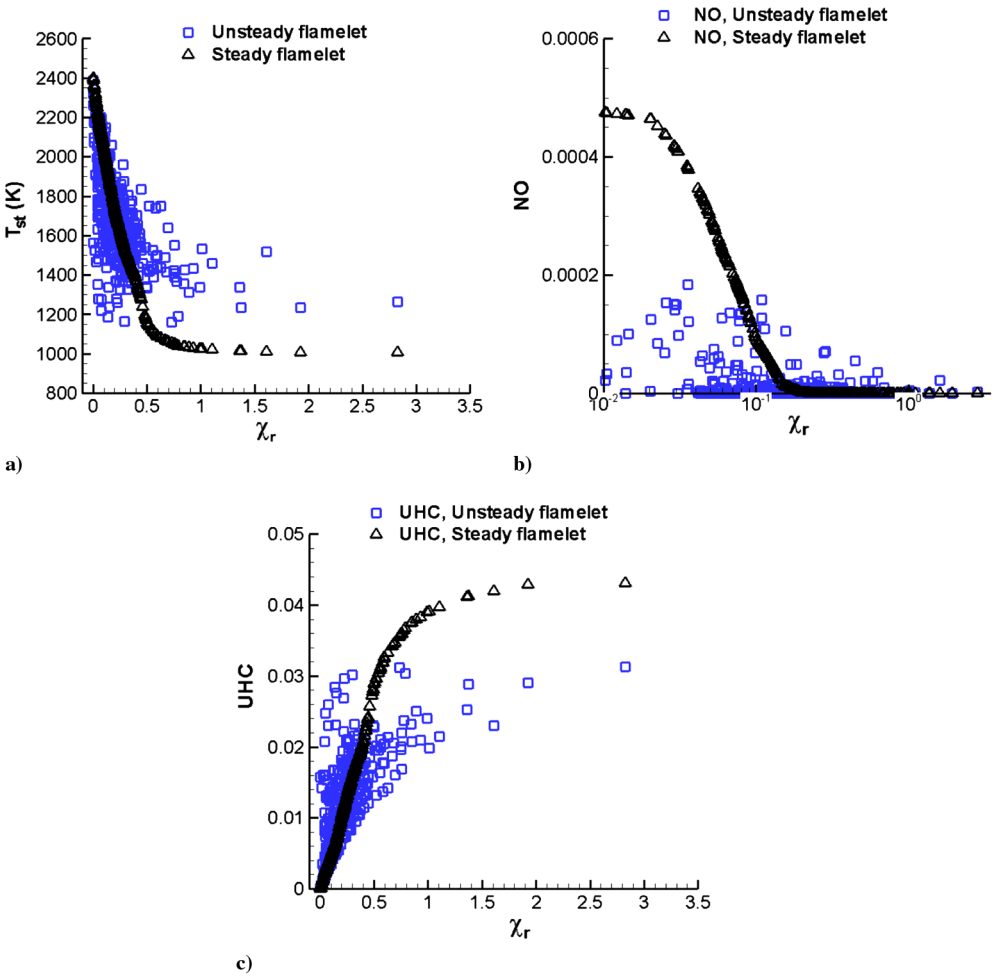

Fig. 17 Unsteady response of T_{st} (K) as a function of a) time and b) χ_r for flamelet history 3 with higher μ and σ using unsteady and steady flamelet models.

We observe from Fig. 17c that UHC mass fractions significantly increase during local extinction events, indicating tradeoffs between UHC and NO formation. This suggests that temporary flame-weakening/flame-recovery events (see Figs. 14a–14c, for instance) may be more favorable than local extinction/reignition events for the simultaneous control of NO and UHC. Essentially, during temporary flame weakening/recovery, whereas NO levels may be lower due to delayed response and phase-lag effects, UHC levels would remain low due to the absence of extinction and the associated high temperatures (greater than 1500 K). Consistent with the faster chemical-response time scales of UHC, we note in Fig. 17c that steady flamelet models perform relatively better with respect to UHC, even though deviations up to 33% are observed in the instantaneous peak values.

To relate the local extinction/reignition events to spatial information in the jet, consider Fig. 18, which shows five time histories of T_{st} represented as a function of axial location in the jet from unsteady flamelet computations employing higher mean and rms values of χ_{st}. We observe local extinction events at upstream axial locations and temporary flame-weakening events beyond $x/d = 14$. For the flamelet histories shown, reignition events are also observed at the upstream locations, indicating that the mean temperature would represent the net effects due to extinction and reignition events. We can then think of flame liftoff height as the location at which there is predominantly extinction and less reignition, so that the mean flame would remain extinguished. Furthermore, these trends are in good qualitative agreement with those reported in Sandia flames E and F [35], in which the probabilities for local extinction and reignition were found to decrease and increase, respectively, with increasing axial locations.

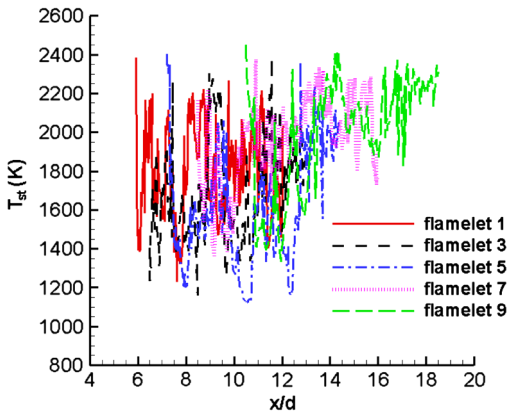

Fig. 18 Temperature T_{st} time histories from unsteady flamelet calculations corresponding to higher-intensity fluctuations represented as a function of axial location in the jet. Only five flamelets are shown for clarity.

Figures 19a and 19b show the computed mean temperature T_{st} and NO mass fraction, respectively, from the 10 flamelet histories with higher-intensity fluctuations as a function of axial location in the jet. Note that in addition to the predictions with unsteady and steady flamelet models, Figs. 19a and 19b show the predictions using a *steady-flamelet/steady-strain* (SFSS) model. Essentially, the SFSS prediction corresponds to the steady flamelet solution at the mean (or steady) value of χ_{st} at each axial location. In other words, the SFSS model results are similar to what one may obtain from a RANS simulation employing a steady flamelet model, in which temporal fluctuations are not taken into account. However, note that the (temporal) mean value of χ_{st} at each axial location is estimated using the time histories generated from LES. Hence, in using this analogy between the SFSS model and RANS results, we are making the implicit assumption that the mean value of χ_{st} is the same, regardless of whether it is computed using RANS or LES. Though this is true in principle, the mean values from RANS and LES may differ depending on factors such as the choice of subgrid-scale models and the selected numerical resolution and filter characteristics in LES. Nevertheless, the analogy between SFSS and RANS is invoked here to merely explore the importance of accounting for the transient flame response to fluctuations of χ_{st}.

We observe from Fig. 19a that the T_{st} predictions from the three models agree within 5% for axial distances considered, indicating that the mean values of T_{st} are not significantly affected, due to instantaneous excursions of χ_{st} above and below χ_e. This trend may be understood by an inspection of Fig. 17a, which shows that whereas the steady flamelet model underestimates T_{st} during extinction (essentially predicts frozen flow temperatures at values of χ_{st} close to χ_e), it overestimates T_{st} during reignition, due to the lack of chemical phase-lag effects. This leads to compensatory effects and mean values close to unsteady flamelet predictions. However, as with the lower-intensity fluctuations, mean NO values would be significantly affected.

We observe from Fig. 19b that the SFSS model grossly underestimates the mean NO mass fraction at $x/d = 12$, whereas the steady flamelet model overestimates NO by about an order of magnitude. These discrepancies between the models indicate that fluctuations of χ_{st} and transient effects on NO response due to extinction/reignition events are relatively significant at upstream jet locations ($x/d < 14$). The agreement between the models improves at downstream jet locations, where the SFSS and steady flamelet models yield somewhat similar values of NO. Hence, in the simulated jet near-field region at higher Reynolds numbers, we may expect unsteady effects to significantly influence NO formation. In addition, as in the case of lower-intensity χ_{st} fluctuations, mean axial profiles of UHC agreed well with all the three models, indicating that mean UHC concentrations are minimally affected by χ_{st} fluctuations and transient effects. We will now clarify the effects of Da on the unsteady flame response through the variation of the fuel temperature.

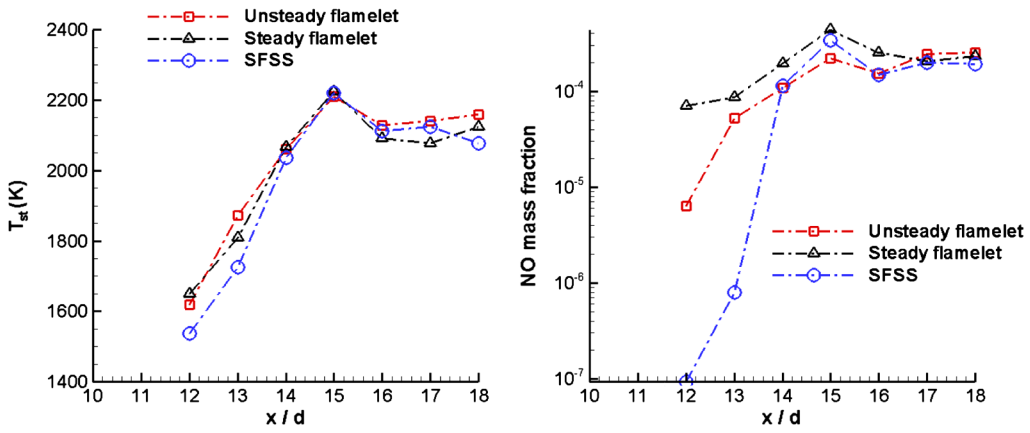

Fig. 19 Mean values of a) T_{st} (K) and b) NO mass fraction computed from the flamelet histories with higher-intensity fluctuations as a function of axial location in the jet.

2. Influence of Da on Unsteady Flame Response

In the discussions so far with $T_{\text{fuel}} = T_a = 1000$ K, we considered relatively strong flames ($Da > 10$), which respond relatively fast to the imposed scalar dissipation rate fluctuations. Hence, the observed unsteady effects on mean temperatures and species mass fractions (except NO) were not very significant. However, with lower fuel temperatures (~400 K) more common in practical applications, the flamelets will respond with longer characteristic time scales, which can in turn result in greater unsteady effects on the temperature and species responses. To explore this possibility, we carried out simulations for flamelets with $T_{\text{fuel}} = 450$ K and subjected them to the time histories with higher mean and rms values. Note that when T_{fuel} is decreased from 1000 to 450 K, the computed steady extinction limit χ_e decreases from about 500 to about 170 s^{-1}. Accordingly, we encounter much greater excursions of χ_{st} above χ_e ($\chi_r \sim 6.0$) for the $T_{\text{fuel}} = 450$ K cases. Moreover, the Da [see Eq. (17)] values for the $T_{\text{fuel}} = 450$ flamelets lie in the range of 1.1–3.5, indicating highly strained flamelets that are closer to extinction. In addition, when $T_{\text{fuel}} = 450$ K, the injected-to-ambient gas density ratio increases to about 8.0 (compared against 3.5 with $T_{\text{fuel}} = 1000$ K), which would lead to higher χ_{st} amplitudes, due to reduced spreading of the jet [5]. Nevertheless, we subject both the $T_{\text{fuel}} = 1000$ and the 450 K flames to similar turbulent time histories to isolate effects due to Da.

Figure 20 shows the mean values of T_{st} computed from the flamelet histories (with higher means and rms) values when $T_{\text{fuel}} = 450$ K. Relative to Fig. 19a, the mean temperature is lower for the lower fuel temperature, indicating the increasing role played by extinction as the fuel temperature decreases (i.e., the flame is weaker). It is interesting that steady flamelet predictions agree well with unsteady flamelets, indicating compensatory effects during extinction and reignition, as in the cases with $T_{\text{fuel}} = 1000$ K, discussed before. However, at $x/d = 12$, the SFSS model predicts an extinguished flame, whereas the steady and unsteady flamelet models result in temperatures that are about 40% higher. This indicates the role of transient flame response to fluctuations of χ_{st} and possible differences in flame liftoff predictions between the models. Hence, for jets with higher global strain rates (U_{inj}/d) and with relatively weak (or strained) flames (i.e., lower Da), fluctuations of the scalar dissipation rate are expected to be important for flame liftoff predictions. Though not shown here, the conclusions discussed before for the $T_{\text{fuel}} = 1000$ K cases with respect to differences between steady and unsteady flamelet models and chemical phase-lag effects on the response of species, such as NO and UHC, were found to be valid with $T_{\text{fuel}} = 450$ K as well. Note, however, that questions related to kinetic effects, such as the role of low-temperature and high-temperature reaction pathways during extinction/reignition in the presence of scalar dissipation rate fluctuations, could be influenced by choices such as the fuel temperature. In the present work, the choice of a relatively high fuel temperature of 1000 K, though relatively high in the context of engine combustion, has minimal effects on the conclusions drawn from the results. Furthermore, because we primarily encounter relatively large strain rates for the extrapolated cases considered here, it is expected that radiative heat losses would be outweighed by strain-induced diffusive losses [60]. Hence, the conclusions drawn with respect to unsteady extinction/reignition, species (such as NO) responses, and liftoff are expected to be valid even when radiative heat losses are included.

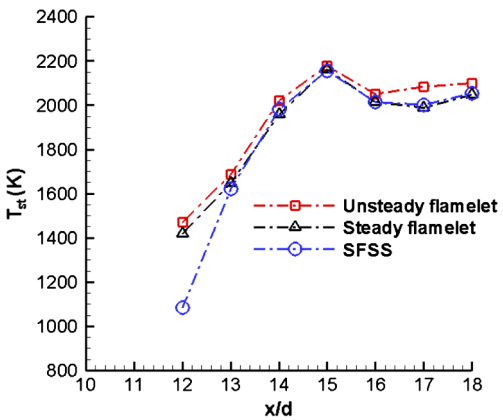

Fig. 20 Mean values of Tst (K) computed from the flamelet histories with higher-intensity fluctuations and $T_{\text{fuel}} = 450$ K as a function of axial location in the jet.

Before we summarize and conclude, it is important to note that the conclusions from the present work regarding the trends in local extinction/reignition and the validity of steady flamelet models pertain to high-Reynolds-number variable-density jets under high pressures and high-temperature conditions. With respect to the nature of scalar dissipation rate fluctuations in the near field of the jet, parameters such as the injected-to-ambient density ratio are expected to have a significant effect. For instance, as we proceed from variable-density to constant-density jets, certain trends in the fluctuating χ_{st} time records, such as relatively short-lived peak values, which are closely linked to the performance of steady flamelet models, may change. Moreover, the flamelets considered here at relatively high pressures and temperatures respond with relatively fast chemical time scales. In the case of laboratory-scale atmospheric flames, such as the Sandia flames [35], the chemical time scales may be much slower, which would affect the validity of steady flamelet models. Clarifications of effects due to the chosen flame characteristics (i.e., pressure and fuel/oxidizer temperatures) and jet characteristics (such as the density ratio) on the unsteady response of flames are interesting and important avenues for future works.

V. Conclusions

In this work, we investigated unsteady effects on the response of laminar diffusion flamelets subjected to turbulent fluctuations of the scalar dissipation rate. These turbulent fluctuations were obtained from the analysis of the near field of a nonreacting 70,000-Reynolds-number variable-density isothermal gas jet computed with LES. A reduced-chemical kinetic mechanism for n-heptane oxidation involving 159 species and 1540 reaction steps was employed. The pressures and temperatures simulated were representative of diesel engine combustion chambers. The unsteady response of the flame temperature, major species (i.e., CO_2 and H_2O), and pollutants (i.e., NO and UHC) was investigated, and the applicability of steady flamelet models was assessed.

The LES formulation employed was validated for the prediction of passive scalar statistics, such as means and variances, through comparisons with available measurements in self-similar jets. The means and fluctuations of the scalar dissipation rates were characterized. To generate fluctuations of χ_{st} that are experienced by the near-field flamelets in the jet, Lagrangian-type tracking of stoichiometric isocontours in space and time was employed. Ten representative flamelet histories were computed and then employed in studies focusing on the unsteady response of diffusion flamelets. However, the effects of combustion heat release on the predicted scalar dissipation rate time histories were ignored. The impact of this assumption on the conclusions has to be assessed in future studies.

The generated flamelet histories involved relatively small means ($\sim 0.06\chi_e$), rms ($\sim 0.06\chi_e$), and peak values ($\sim 0.3\chi_e$) and relatively large mean Damköhler numbers (~15–50), and so temporary flame-weakening events followed by flame recovery were observed in the jet near-field region. The unsteady flame response was also compared with predictions from a steady flamelet library corresponding to the instantaneous χ_{st} values from the turbulent time records. The comparisons showed good agreement between the unsteady and steady flamelet models with respect to the mean temperature, mean major species (i.e., CO_2 and H_2O), mass fractions, and mean UHC mass fractions. However, deviations up to 20% were observed in the mean NO mass fraction due to the inability of steady flamelet models to describe the delayed response of NO (i.e., phase-lag effects) during flame-weakening/recovery events.

To understand the possible behavior in jets with higher global strain rates occurring in diesel chambers, we considered flamelet

histories with higher means and rms values than those computed for the 70,000-Reynolds-number jet. In these cases, transient local extinction/reignition events were observed, which can be described by unsteady-flamelet/progress-variable models from a modeling standpoint. In addition, extinction events increase in importance as weaker flames (i.e., with a fuel temperature of 450 K, resulting in lower Damköhler numbers) are considered. The extinction/reignition events significantly suppress NO formation, due to reduced mixing and residence times and the associated chemical phase-lag effects. In contrast, UHC levels were found to increase, due to extinction events and faster recovery following reignition. This tradeoff between NO and UHC suggested that temporary flame-weakening/recovery events may be more favorable than local extinction/reignition events for the simultaneous control of these pollutants.

Steady flamelet models were found to significantly underestimate the temperatures during extinction and to overestimate the temperatures during reignition. Because of these compensatory effects, the mean temperatures with steady and unsteady flamelet models agreed well. However, the failure of steady flamelet models to describe transient extinction/reignition had a drastic effect on instantaneous and mean NO mass fractions, leading to deviations more than an order of magnitude at upstream jet locations (e.g., $x/d = 12$). Hence, the present results indicate that although steady flamelet models in the context of LES (i.e., accounting for χ_{st} fluctuations but not chemical phase-lag effects) may be reasonable for the predictions of mean temperatures, major species, and UHCs, unsteady flamelets (which account for both χ_{st} fluctuations and chemical phase-lag effects) will be needed for mean NO predictions.

The analysis of flame response to turbulent time records with higher means and rms values showed that unsteady extinction/reignition events may be associated with phenomena such as flame liftoff. Based on the present results, flame liftoff in the jet can occur at the location at which multiple flamelet histories predominantly lead to extinction, with low probabilities for reignition. This would result in the mean flame being extinguished at the liftoff location. Comparisons of unsteady and steady flamelet predictions with a steady-flamelet/steady-strain (SFSS) model showed that accounting for the transient flame response to fluctuations of the scalar dissipation rate is important in predictions of near-field phenomena in high-Reynolds-number jets.

Acknowledgments

Computing resources for this work were provided by the National Center for Supercomputing Applications (NCSA) on the NCSA Xeon cluster under grant number MCAO6N038. Vinicio Magi developed the original version of the FLEDS code employed in this work. The authors thank him for useful discussions during the course of this study. The authors thank Lyle Pickett at Sandia National Laboratories for useful discussions on transient liftoff-related phenomena in diesel jets.

References

[1] Peters, N., *Turbulent Combustion*, Cambridge Univ. Press, Cambridge, England, U.K., 2000.

[2] Veynante, D., and Vervisch, L., "Turbulent Combustion Modeling," *Progress in Energy and Combustion Science*, Vol. 28, No. 3, 2002, pp. 193–266. doi:10.1016/S0360-1285(01)00017-X

[3] Siebers, D. L., Higgins, B. S., and Pickett, L. M., "Flame Liftoff on Direct-Injection Diesel Fuel Jets: Oxygen Concentration Effects," Society of Automotive Engineers Paper 2002-01-0890, 2002.

[4] Pickett, L. M., and Siebers, D. L., "Soot in Diesel Fuel Jets: Effects of Ambient Temperature, Ambient Density, and Injection Pressure," *Combustion and Flame*, Vol. 138, Nos. 1–2, 2004, pp. 114–135. doi:10.1016/j.combustflame.2004.04.006

[5] Venugopal, R., and Abraham, J., "A Numerical Investigation of Flame Liftoff in Diesel Jets," *Combustion Science and Technology*, Vol. 179, No. 12, 2007, pp. 2599–2618. doi:10.1080/00102200701487095

[6] Senecal, P. K., Pomraning, E., and Richards, K. J., "Multidimensional Modeling of Direct-Injection Diesel Spray Liquid Length and Flame Liftoff Length Using CFD and Parallel Detailed Chemistry," Society of Automotive Engineers Paper 2003-01-1043, 2003.

[7] Pickett, L. M., Kook, S., Persson, H., and Andersson, O., "Diesel Fuel Jet Liftoff Stabilization in the Presence of Laser-Induced Plasma Ignition," *Proceedings of the Combustion Institute*, Vol. 32, (to be published).

[8] Agarwal, S. K., "A Review of Spray Ignition Phenomena: Present Status and Future Research," *Progress in Energy and Combustion Science*, Vol. 24, No. 6, 1998, pp. 565–600. doi:10.1016/S0360-1285(98)00016-1

[9] Vervisch, L., and Poinsot, T., "Direct Numerical Simulation of Non-Premixed Turbulent Flames," *Annual Review of Fluid Mechanics*, Jan. 1998, pp. 655–691. doi:10.1146/annurev.fluid.30.1.655

[10] Pantano, C., Sarkar, S., and Williams, F. A., "Mixing of a Conserved Scalar in a Turbulent Reacting Shear Layer," *Journal of Fluid Mechanics*, Vol. 481, Apr. 2003, pp. 291–328. doi:10.1017/S0022112003003872

[11] Geyer, D., Kempf, A., Dreizler, J., and Janicka, J., "Scalar Dissipation Rates in Isothermal and Reactive Turbulent Opposed-Jets: 1-D Raman/Rayleigh Experiments Supported by LES," *Proceedings of the Combustion Institute*, Vol. 30, No. 1, 2005, pp. 681–689. doi:10.1016/j.proci.2004.08.216

[12] Pitsch, H., and Steiner, H., "Scalar Mixing and Dissipation Rate in Large-Eddy Simulations of Non-Premixed Turbulent Combustion," *Twenty-Eighth Symposium (International) on Combustion*, Vol. 1, Combustion Inst., Pittsburgh, PA, 2000, pp. 41–49.

[13] Broadwell, J. E., Dahm, W. J. A., and Mungal, M., "Blowout of Turbulent Diffusion Flames," *Twentieth Symposium (International) on Combustion*, Combustion Inst., Pittsburgh, PA, 1985, pp. 303–310.

[14] Pitts, W. M., "Importance of Isothermal Mixing Processes in the Understanding of Liftoff and Blowout of Turbulent Jet Diffusion Flames," *Combustion and Flame*, Vol. 76, No. 2, 1989, pp. 197–212. doi:10.1016/0010-2180(89)90067-9

[15] Richards, C. D., and Pitts, W. M., "Global Density Effects on the Self-Preservation Behavior of Turbulent Free Jets," *Journal of Fluid Mechanics*, Vol. 254, Sept. 1993, pp. 417–435. doi:10.1017/S0022112093002204

[16] Pitts, W. M., and Kashiwagi, T., "The Application of Laser-induced Rayleigh Light Scattering in the Study of Turbulent Mixing," *Journal of Fluid Mechanics*, Vol. 141, Apr. 1984, pp. 391–429. doi:10.1017/S0022112084000902

[17] Namazian, M., Schefer, W., and Kelly, J., "Scalar Dissipation Rate Measurements in the Developing Region of a Jet," *Combustion and Flame*, Vol. 74, No. 2, 1988, pp. 147–160. doi:10.1016/0010-2180(88)90013-2

[18] Effelsberg, E., and Peters, N., "Scalar Dissipation Rates in Turbulent Jets and Jet Diffusion Flames," *Twenty-Second Symposium (International) on Combustion*, Combustion Inst., Pittsburgh, PA, 1989, pp. 693–700.

[19] Oefelein, J., "Large-Eddy Simulation of Turbulent Combustion Processes in Propulsion and Power Systems," *Progress in Aerospace Sciences*, Vol. 42, No. 1, 2006, pp. 2–37.

[20] Meneveau, C., and Katz, J., "Scalar-Invariance and Turbulence Models for Large Eddy Simulation," *Annual Review of Fluid Mechanics*, Vol. 32, Jan. 2000, pp. 1–32. doi:10.1146/annurev.fluid.32.1.1

[21] Pitsch, H., "Large-Eddy Simulation of Turbulent Combustion," *Annual Review of Fluid Mechanics*, Vol. 38, Jan. 2006, pp. 453–482. doi:10.1146/annurev.fluid.38.050304.092133

[22] DeBonius, J. R., and Scott, J. N., "Large-Eddy Simulation of a Turbulent Compressible Round Jet," *AIAA Journal*, Vol. 40, No. 7, 2002, pp. 1346–1354. doi:10.2514/2.1794

[23] Bogey, C., Bailley, C., and Juve, D., "Noise Investigation in a High Subsonic Moderate Reynolds Number Jet Using a Compressible Large Eddy Simulation," *Theoretical and Computational Fluid Dynamics*, Vol. 16, No. 4, 2003, pp. 273–297. doi:10.1007/s00162-002-0079-4

[24] Ribault, C. L., Sarkar, S., and Stanley, S. A., "Large Eddy Simulation of Evolution of Passive Scalar in a Plane Jet," *AIAA Journal*, Vol. 39, No. 8, 2001, pp. 1509–1516. doi:10.2514/2.1475

[25] Anders, J. W., Magi, V., and Abraham, J., "Large-Eddy Simulation in the Near Field of a Transient Multicomponent Gas Jet with Density Gradients," *Computers and Fluids*, Vol. 36, No. 10, 2007, pp. 1609–1620. doi:10.1016/j.compfluid.2007.03.002

[26] Egolfopoulos, F. N., and Campbell, C. S., "Unsteady Counterflowing

Strained Diffusion Flames: Diffusion-limited Frequency Response," *Journal of Fluid Mechanics*, Vol. 318, July 1996, pp. 1–29. doi:10.1017/S0022112096007008

[27] Im, H. G., Chen, J. H., and Chen, J. -Y., "Chemical Response of Methane/Air Diffusion Flames to Unsteady Strain Rate," *Combustion and Flame*, Vol. 118, Nos. 1–2, 1999, pp. 204–212. doi:10.1016/S0010-2180(98)00153-9

[28] Welle, E. J., Roberts, W. L., Carter, C. D., and Donbar, J. M., "The Response of a Counter-Flow Diffusion Flame Subjected to a Transient Flow Field," *Combustion and Flame*, Vol. 135, No. 3, 2003, pp. 285–297. doi:10.1016/S0010-2180(03)00167-6

[29] Im, H. G., Law, C. K., Kim, J. S., and Williams, F. A., "Response of Counterflow Diffusion Flames to Oscillating Strain Rates," *Combustion and Flame*, Vol. 100, Nos. 1–2, 1995, pp. 21–30. doi:10.1016/0010-2180(94)00059-2

[30] Kistler, J. S., Sung, C. J., Kreutz, T. G., and Law, C. K., "Extinction of Counterflow Diffusion Flames Under Velocity Oscillations," *Twenty-Sixth Symposium (International) on Combustion*, Combustion Inst., Pittsburgh, PA, 1996, pp. 113–120.

[31] Santoro, V. S., Kyritsis, D. C., Linan, A., and Gomez, A., "Vortex-induced Extinction Behavior in Methanol Gaseous Flames: A Comparison with Quasi-Steady Extinction," *Twenty-Eighth Symposium (International) on Combustion*, Vol. 2, Combustion Inst., Pittsburgh, PA, 2000, pp. 2109–2116.

[32] Oh, C. B., Lee, C. E., and Park, J., "Numerical Investigation of Extinction in a Counterflow Non-Premixed Flame Perturbed by a Vortex," *Combustion and Flame*, Vol. 138, No. 3, 2004, pp. 225–241. doi:10.1016/j.combustflame.2004.03.013

[33] Venugopal, R., and Abraham, J., "A 2-D DNS Investigation of Extinction and Reignition Dynamics in Non-Premixed Flame-Vortex Interactions," *Combustion and Flame*, Vol. 153, No. 3, 2008, pp. 442–464. doi:10.1016/j.combustflame.2007.10.021

[34] Pitsch, H., "Improved Pollutant Predictions in Large-Eddy Simulations of Turbulent Non-Premixed Combustion by Considering Scalar Dissipation Rate Fluctuations," *Proceedings of the Combustion Institute*, Vol. 29, No. 2, 2002, pp. 1971–1978. doi:10.1016/S1540-7489(02)80240-1

[35] Barlow, R. S., and Frank, J. H., "Effects of Turbulence on Species Mass Fractions in Methane/Air Jet Flames," *Twenty-Seventh Symposium (International) on Combustion*, Combustion Inst., Pittsburgh, PA, 1998, pp. 1087–1095.

[36] Peters, N., and Williams, F. A., "Liftoff Characteristics of Turbulent Jet Diffusion Flames," *AIAA Journal*, Vol. 21, No. 3, 1983, pp. 423–429. doi:10.2514/3.8089

[37] Sripakagorn, P., Mitarai, S., Kosaly, G., and Pitsch, H., "Extinction and Reignition in a Diffusion Flame: A Direct Numerical Simulation Study," *Journal of Fluid Mechanics*, Vol. 518, Nov. 2004, pp. 231–259. doi:10.1017/S0022112004001004

[38] Venugopal, R., and Abraham, J., "Numerical Investigations of Reignition in Vortex-Perturbed *n*-Heptane Nonpremixed Flames," *AIAA Journal*, Vol. 46, No. 10, 2008, pp. 2479–2497. doi:10.2514/1.35094

[39] Santoro, V. S., Linan, A., and Gomez, A., "Propagation of Edge Flames in Counterflow Mixing Layers: Experiments and Theory," *Twenty-Eighth Symposium (International) on Combustion*, Vol. 2, Combustion Inst., Pittsburgh, PA, 2000, 2039–2046.

[40] Amantini, G., Frank, J. H., and Gomez, A., "Experiments on Standing and Traveling Edge Flames Around Flame Holes," *Proceedings of the Combustion Institute*, Vol. 30, No. 1, 2005, pp. 313–321. doi:10.1016/j.proci.2004.08.230

[41] Hermanns, M., Vega, M., and Linan, A., "On the Dynamics of Flame-edges in Diffusion-flame/Vortex Interactions," *Combustion and Flame*, Vol. 149, Nos. 1–2, 2007, pp. 32–48. doi:10.1016/j.combustflame.2006.12.012

[42] Pantano, C., "Direct Simulation of Non-Premixed Flame Extinction in a Methane-air Jet with Reduced Chemistry," *Journal of Fluid Mechanics*, Vol. 514, Sept. 2004, pp. 231–270. doi:10.1017/S0022112004000266

[43] Hawkes, E. R., Sankaran, R., Sutherland, J. C., and Chen, J. H., "Scalar Mixing in Direct Numerical Simulations of Temporally Evolving Plane Jet Flames with Skeletal CO/H_2 Kinetics," *Proceedings of the Combustion Institute*, Vol. 31, No. 1, 2007, pp. 1633–1640. doi:10.1016/j.proci.2006.08.079

[44] Abraham, J., and Magi, V., "Exploring Velocity and Density Ratio Effects in a Mixing Layer Using DNS," *International Journal of Computational Fluid Dynamics*, Vol. 8, No. 2, 1997, pp. 147–151. doi:10.1080/10618569708940801

[45] Viggiano, A., and Magi, V., "A 2-D Investigation of *n*-Heptane Autoignition by Means of Direct Numerical Simulation," *Combustion and Flame*, Vol. 137, No. 4, 2004, pp. 432–443. doi:10.1016/j.combustflame.2004.03.003

[46] Lele, S. K., "Compact Finite Difference Schemes with Spectral-Like Resolution," *Journal of Computational Physics*, Vol. 103, No. 1, 1992, pp. 16–42. doi:10.1016/0021-9991(92)90324-R

[47] Carnahan, B., *Applied Numerical Methods*, Wiley, New York, 1969, p. 363.

[48] Poinsot, T. J., and Lele, S. K., "Boundary Conditions for Direct Simulations of Compressible Viscous Flows," *Journal of Computational Physics*, Vol. 101, No. 1, 1992, pp. 104–129. doi:10.1016/0021-9991(92)90046-2

[49] Uzun, A., "3-D Large-Eddy Simulation for Jet Aeroacoustics," Ph.D. Thesis, Purdue Univ., West Lafayette, IN, Dec. 2003.

[50] Pope, S. B., *Turbulent Flows*, Cambridge Univ. Press, Cambridge, England, U.K., 2000, pp. 119–122.

[51] Anders, J. W., "Turbulence and Residual Gas Effects in Pulsed Diesel Jets," Ph.D. Thesis, Purdue Univ., West Lafayette, IN, Aug. 2006.

[52] Abraham, J., "Entrainment Characteristics of Transient Gas Jets," *Numerical Heat Transfer, Part A, Applications*, Vol. 30, No. 4, 1996, pp. 347–364. doi:10.1080/10407789608913844

[53] Schefer, R. W., and Dibble, R. W., "Mixture Fraction in a Turbulent Non-Reacting Propane Jet," *AIAA Journal*, Vol. 39, No. 1, 2001, pp. 64–72. doi:10.2514/2.1271

[54] Peters, N., "Laminar Diffusion Flamelet Models in Non-Premixed Turbulent Combustion," *Progress in Energy and Combustion Science*, Vol. 10, No. 3, 1984, pp. 319–339. doi:10.1016/0360-1285(84)90114-X

[55] Gopalakrishnan, V., and Abraham, J., "An Investigation of Ignition Behavior in Diesel Sprays," *Proceedings of the Combustion Institute*, Vol. 29, No. 1, 2002, pp. 641–646. doi:10.1016/S1540-7489(02)80082-7

[56] Gopalakrishnan, V., and Abraham, J., "Computed NO and Soot Distribution in Turbulent Transient Jets under Diesel Conditions," *Combustion Science and Technology*, Vol. 176, No. 4, 2004, pp. 603–641. doi:10.1080/00102200490276818

[57] Seiser, R., Pitsch, H., Seshadri, K., Pitz, W. J., and Curran, H. J., "Extinction and Autoignition of *n*-Heptane in Counterflow Configuration," *Twenty-Eighth Symposium (International) on Combustion*, Vol. 2, Combustion Inst., Pittsburgh, PA, 2000, pp. 2029–2037.

[58] Bushe, W. K., and Steiner, H., "Conditional Moment Closure for Large Eddy Simulation of Nonpremixed Turbulent Reacting Flows," *Physics of Fluids*, Vol. 11, July 1999, pp. 1896–1906. doi:10.1063/1.870052

[59] Wall, C., Boersma, B., and Moin, P., "An Evaluation of the Assumed Beta Probability Density Function Subgrid-Scale Model for Large-Eddy Simulation of Non-Premixed Turbulent Combustion with Heat Release," *Physics of Fluids*, Vol. 12, Oct. 2000, pp. 2522–2529. doi:10.1063/1.1287911

[60] Williams, F. A., "Progress in Knowledge of Flamelet Structure and Extinction," *Progress in Energy and Combustion Science*, Vol. 26, Aug. 2000, pp. 657–682. doi:10.1016/S0360-1285(00)00012-5

[61] Law, C. K., *Combustion Physics*, Cambridge Univ. Press, Cambridge, England, U.K., 2000.

[62] Safta, C., Enachescu, S., and Madnia, C. K., "Interaction of a Vortex Ring with a Diffusion Flame," *Physics of Fluids*, Vol. 14, Feb. 2002, pp. 668–681. doi:10.1063/1.1429248

[63] Pierce, C. D., and Moin, P., "Progress-Variable Approach for Large-Eddy Simulation of Non-Premixed Turbulent Combustion," *Journal of Fluid Mechanics*, Vol. 504, Apr. 2004, pp. 73–97. doi:10.1017/S0022112004008213

[64] Pitsch, H., and Ihme, M., "An Unsteady Flamelet/Progress Variable Method for LES of Non-Premixed Turbulent Combustion," 43rd AIAA Aerospace Sciences Meeting and Exhibit, AIAA Paper 2004-557, Reno, NV, Jan. 2005.

[65] Heywood, J. B., *Internal Combustion Engine Fundamentals*, McGraw–Hill, New York, 1988.

T. Jackson
Associate Editor